JOURNAL OF
REINFORCED
PLASTICS &
COMPOSITES

Original article

Journal of Reinforced Plastics and Composites
2022, Vol. 41(17-18) 679–704

DOI: 10.1177/07316844211068116
journals.sagepub.com/home/jrp
SAGE

Prediction of compressive strength of fiber-reinforced polymers-confined cylindrical concrete using artificial intelligence methods

Faride Jamali[1], Seyed Roohollah Mousavi[1], Abdolhamid Bahr Peyma[1] and Yaser Moodi[1]

Abstract

Compressive strength is the ability of materials to withstand loads without deformation or cracking. It is one of the most important criteria for evaluating the properties of concrete. The use of Fiber-Reinforced Polymers (FRP) to Strengthen concrete columns and as a supplement to improve some properties of concrete materials has received much attention in recent decades. Therefore, it is important to investigate and determine the compressive strength of confined concrete with FRP sheets. In this study, a comprehensive database containing 1066 specimens of concrete cylinders confined with FRP sheets has been collected. Then, using machine learning methods, the estimation and evaluation of the compressive strength of the mentioned specimens were discussed. The artificial neural network of multilayer perceptron (MLP) and support vector regression (SVR), fuzzy neural inference system (ANFIS), and its combination with particle swarm algorithm (PSO) and kriging interpolation method are the methods used in this study. Subsequently, these methods were compared with the models presented in previous studies. The results of this comparison show that the kriging interpolation method with a correlation coefficient of 0.985 in estimating compressive strength has the lowest error compared to other models.

Keywords

compressive strength, fiber-reinforced polymer, concrete cylinder, artificial intelligence

Introduction

The use of fiber-reinforced polymers (FRP) enhances the compressive strength of columns and increases their ductility. FRP were first used in the mid-1980s to strengthen existing reinforced concrete columns against seismic loads.[1] During the last two decades, many experimental and analytical studies have been performed on concrete cylindrical specimens confined with FRP sheets. The results of these studies have confirmed the effectiveness of FRP sheets in increasing compressive strength and ductility. Experimental and analytical studies in this field include the laboratory study of Fardis et al.[2] in 1982. Experimental studies by Rousakis et al.[3] in 2001 and Nani et al.[4] In 1995 have also shown that the twisting of FRP sheets strengthens the compressive strength and ductility of concrete specimens. Also, many stress–strain models have been proposed to estimate and simulate laboratory results. In 1988, Mander et al.[5] proposed a model for estimating the ultimate compressive strength and strain of confined concrete with FRP. Pham et al.[6] in 2013, Lam et al. In 2003,[7] Rousakis et al. In 2003 [8] presented stress–strain models to estimate and simulate laboratory results. In 2015, Sadeghian and Pham[9] performed an analysis on 518 laboratory specimens. Considering the actual rupture strain of the confinement, they presented a model for estimating the compressive strength of FRP-confined concrete cylinders. Ozbakkaloglu et al.[10] In 2013 investigated the effect of various parameters on the behavior of concrete. They developed a model that improved the compressive strength and the final axial strain of FRP-confined concrete. Keshtegar et al.[11] developed two nonlinear empirical models for accurate prediction of the FRP-confined concrete segments with two optimization approaches which are used for determining the unknown coefficients of nonlinear models named dynamical harmony search[11] and gradient method-based chaos control.[12]

[1]Civil Engineering Department, University of Sistan and Baluchestan, Zahedan, Iran

Corresponding author:
Seyed Roohollah Mousavi, Civil Engineering Department, University of Sistan and Baluchestan, Daneshgah Street, Zahedan 98155-987, Iran.
Email: s.r.mousavi@eng.usb.ac.ir

Recently, the hybrid artificial intelligent model given from two calibrating approaches is extended by Keshtegar et al.[13–16] named as response surface method (RSM) combined by support vector regression (RSM-SVR). The RSM-SVR method is performed by two machine learning approaches as RSM applied for connection between input variables and data handing sets as input for regression support vector machines (SVR) in the first stage and SVR applied for main models for a nonlinear relation between data handling sets provided by RSM and output responses. This method has acceptable application for concrete structures as the predictions performances of the ultimate condition in FRP-confined concrete,[13] shear capacity of steel fiber-unconfined concrete beams,[14] a shear load of reinforced concrete walls,[15] and reinforcing bar development length.[16] Recently, Seghier et al.[17,18] developed the hybrid method of SVR combined with optimization approaches such as Genetic Algorithm (GA), particle swarm algorithm (PSO) and Whale Optimization Algorithm (WOA) and these models are applied for the prediction of the ultimate condition of concrete segment warped by FRP sheets.[18] Seghier et al.[19] are applied the machine learning approaches for predicting maximum pitting corrosion depth of pipes. In this current work, the authors introduced several machine learning approaches which are compared with empirical models for both accuracy and tendency.

Today and in recent decades, the use of artificial intelligence methods has become popular. ML (machine learning) is used for optimization, estimation, etc. purposes. One of the applications of ML is to use them to determine the pattern and relationship between statistical and laboratory data. The purpose of these new methods of prediction is to minimize the difference between laboratory data and predicted data on various issues.

In 2014, Pham et al.[20] used artificial neural networks to predict the compressive strength and strain of cubic concrete specimens confined with FRP. In 2010, Sobhani et al.[21] used artificial neural networks (ANN), adaptive fuzzy neural inference system (ANFIS), and regression analysis to predict the compressive strength of concrete without slump. In 2019, Moodi et al.[22] proposed a modified model for determining the compressive strength of concrete confined with FRP sheets in circular sections using a genetic optimization algorithm; In their proposed models, FRP strain efficiency factor (FRP) is considered as a function of strain ratio, confinement stiffness ratio, and a combination of the two. Also in 2020, Kamgar et al.[23] used a soft calculation method to estimate the compressive strength of confined concrete cylindrical specimens using a set of experimental data. Using a back-propagation feed-forward neural network (FFBPNN), they proposed a new formula for predicting the compressive strength of confined concrete cylinders. The experimental and analytical models presented in previous studies can be more accurately analyzed to estimate the compressive strength of FRP-confined concrete. The application of nonlinear models with flexible relations is the main challenge for artificial intelligent models. The nonlinear effects between input variables and output relation may be neglected in the empirical models while they are simple for application in design codes. The accuracy and robust prediction are also one of the main contributions of the artificial intelligent-based models. Therefore, considering the mechanical and geometric properties such as diameter and height of the cylinder, compressive strength, and modulus of elasticity of Unconfined concrete, tensile strength, modulus of elasticity, thickness, and several turns of FRP sheet as input parameters, compressive strength is predicted. The results show less error of the Kriging interpolation method with a correlation coefficient of 0.985 in estimating compressive strength. Also, Table 1 shows the details of research conducted with different methods of artificial intelligence. These details include the number of specimens, the method used, and the type of section.

In this study, 1066 experimental specimens of FRP-confined concrete cylinders were collected from previous researches. A large number of specimens has created a comprehensive database. Then, a complete method with a minimum difference for estimating the compressive strength of FRP-confined concrete cylinders is presented. Multilayer perceptron artificial neural network (MLP) and SVR, ANFIS, and its combination with PSO and kriging interpolation method are the methods used in this research.

Experimental dataset used

Given the extensive experiments performed on FRP-confined concrete, this study includes a statistical population of 1066 FRP-confined concrete cylinder specimens collected from previous research. The specifications of the specimens are given in Table 2 of the Appendix. The collected specimens have a diameter (D) and height (H) in the range of 47–406.4 mm and 100–812.5 mm with average values of 145.51 and 297.65 mm, respectively. The compressive strength of the unconfined cylinder (f_{c_0}) is in the range of 6.2–204 MPa with an average value of 53.255 MPa. The FRPs used in this data are CFRP, AFRP, GFRP, and HM-CFRP which their modulus of elasticity (E_f) is from 4.9 to 640 GPa with an average of 174.76 and their tensile strength (F_f) is in the range 75–4900 MPa with an average value of 2707.03 MPa and their thickness (t) is 0.075–15 mm with an average value of 0.825 mm. One-direct FRP covering was also used to confined the specimens in a circular direction. 70% of the data were used for training and 30% for evaluating methods at random. These data are used to estimate and simulate compressive strength by the mentioned methods. Appendix Table A1 in the appendix and Table 2 show the statistical characteristics and the details of the specimens, respectively.

Analytical models of the past researchers

Some researchers have in the past offered relationships to predict the compressive strength of FRP-confined concrete cylinder specimens. The effect of confinement on FRP-confined concrete is shown in Figure 1.

Table 1. Methods used to estimate the compressive strength of FRP-confined columns.

	Study	Year	Section(s)	Method(s)	Number of specimens
1	Cevik and Cabalar [24]	2008	Circular	GP	180
2	Cevik and Guzelbey [25]	2008	Circular	ANN	101
3	Gandomi et al.[26]	2010	Circular	LGP	101
4	Naderpour et al.[27]	2010	Circular	ANN-BP	213
5	Cevik et al.[28]	2010	Circular	GP, SR	101
6	Cevik [29]	2011	Circular	GP, SR, NF, ANN	180
7	Elsanadedy et al.[30]	2012	Circular	ANN	272
8	Jalal and Ramezanianpour[31]	2012	Circular	ANN	128
9	Jalal et al.[32]	2013	Circular	GP, ANFIS	128
10	Lim et al.[33]	2016	Circular	GP	832
11	Mansouri et al.[34]	2016	Circular	ANN, ANFIS MARS, M5Tree	1153
12	Mozumder et al.[35]	2016	Circular	SVR	238
13	Cascardi et al.[36]	2017	Circular	ANN	465
14	Mansouri et al.[37]	2017	Circular	RBNN, ANFIS-SC ANFIS-FCM, M5Tree	519
15	Kamgar et al.[23]	2020	Circular	FFBPNN	281
16	Ahmad et al.[38]	2020	Circular	ANN	708
17	Keshtegar et al.[13]	2021	Circular	RSM-SVR	780

Table 2. Statistical indicators related to variables.

Variables	Min	Max	Standard deviation	Coefficient of variation	
Inputs	f_{c0}(MPa)-unconfined ultimate concrete strength	6.2	204	34.398	0.645
	H (mm) - Height	100	812.8	111.571	0.374
	D(mm) - Diameter	47	406.4	53.435	0.367
	E_f (GPa) - Modulus of elasticity of FRP	4.9	640	112.87	0.645
	F_f(MPa) - Tensile strength of FRP	75	4900	1306.53	0.482
	t (mm) - Thickness of FRP	0.057	15	1.185	1.435
Output	f_{cc} (MPa) - Confined ultimate compressive strength	17.8	381	50.065	0.539

Regardless of the tangential stresses in the longitudinal direction of the column specimen and according to the balance of stresses on the retaining material, the confining pressure $(f_{l,a})$ can be calculated as follows

$$f_{l,a} = \frac{2t_j f_{frp}}{D} = \frac{2E_{frp}\varepsilon_{h,rup}t_j}{D} \quad (1)$$

In the above relation, D is the diameter of the specimen; E_{frp} is the elastic modulus of FRP materials; tj is FRP twist thickness; and $\varepsilon_{h,rup}$ the actual strain of FRP rupture is in the circular direction and is defined as follows.

$$\varepsilon_{h,rup} = k_e\varepsilon_{frp} \quad (2)$$

ε_{FRP} is the ultimate tensile strain of FRP material and the effective strain factor. These studies considered the effect of FRP and parameters such as concrete cylinder diameter, compressive strength of unconfined concrete, FRP modulus of elasticity, FRP rupture strain, and its thickness and based on linear and nonlinear regression methods. To compare soft computational methods with previous models, these models are presented in Table 3 with model descriptions.

Artificial intelligence methods

Brief on fuzzy system theory

The theory of fuzzy sets was first proposed by Professor Lotfi a.zadeh.[46] The most important aspect of fuzzy logic is the ability to express and describe the uncertainty of a parametric or structural type. It is also a new tool for solving problems for which probability theory has no way. The fuzzy inference system creates a nonlinear mapping between input and output, in other words, it processes the input using a set of rules and converts it to output. A membership function can be defined for each input or output. Membership functions are functions that map the membership value (between 0 and 1) of each point in the input space.[46] Figure 2 shows the steps of a fuzzy system and the membership functions used in this research

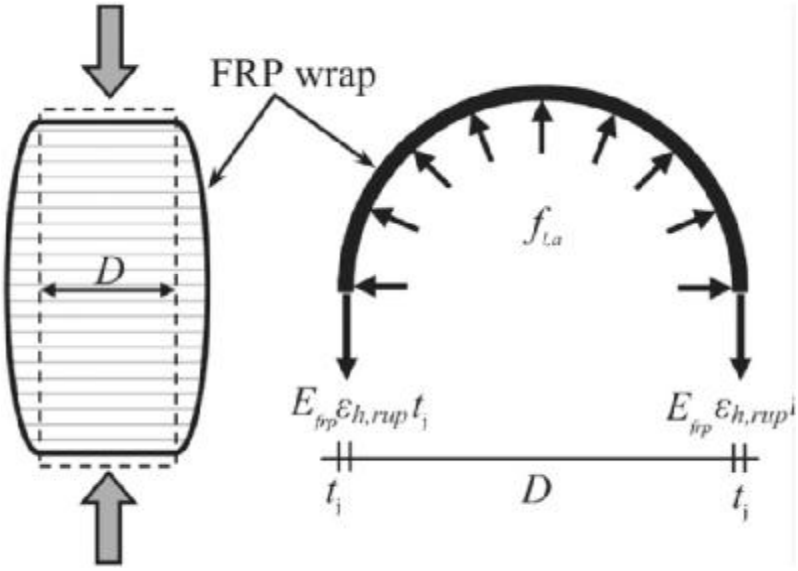

Figure 1. Confinement mechanism in FRP-confined concrete.[9]

The fuzzy system used in this research is the Mamdani system. Due to the visual and interpretive nature of the rules, this system can be widely used in decision support systems and is also implemented as multi-input and multi-output and multi-input and single-output.[49]

Fuzzy neural inference system fuzzy neural system

In 1993, Jang first introduced the fuzzy neural model by combining artificial neural networks and fuzzy systems. ANFIS is trained with the help of an input and output database and then, by creating a fuzzy system (FIS), enables the prediction and estimation of various phenomena in various sciences. Figure 3 and 4, shows the flowchart of a ANFIS and PSO process.[50]

Combining the fuzzy system with the particle swarm algorithm

In this part, the classic training algorithm of the Mamdani system has been replaced by the particle swarm algorithm, which is one of the optimal intelligent algorithms. PSO is one of the optimization algorithms that operate based on random production of the initial population. Each member in this group is defined by the velocity vector and the position vector in the search space. The motion of a particle is guided by the velocity of that particle, and finally, by finding the best value of velocity and location for each particle, their values are updated using the following relations[52]

$$\mathrm{V}(\mathrm{t}+1) = \mathrm{V}(\mathrm{t}) + \mathrm{C1}^{*}\mathrm{rand}(\mathrm{t})^{*}(\mathrm{pbest}(\mathrm{t}) - \mathrm{Position}(\mathrm{t})) + \mathrm{C2}^{*}\mathrm{rand}(\mathrm{t})^{*}(\mathrm{gbest}(\mathrm{t}) - \mathrm{Position}(\mathrm{t1})) \quad (3)$$

$$\mathrm{Position}(\mathrm{t}+1) = \mathrm{Position}(\mathrm{t}) + \mathrm{V}(\mathrm{t}+1) \quad (4)$$

Artificial neural networks

Artificial neural networks are models inspired by the neural structure of the human brain, which is composed of a large number of neurons to process information and solve various problems. The neural network is trained using real data and its output is guided to achieve the set goal. Activator functions are mathematical operators that allow a specific neuron to be activated in the network. Figure 5 shows a simple model of the neural network and transmission functions used in this study.

In training a neural network, by finding the appropriate weight vector (w), bias vector, and minimizing the pre-determined error, the network output approaches the target. In this research, the Levenberg–Marquardt algorithm is used, which is a fast and reliable method based on Newton's classical algorithm.

Regression support vector machines

Support vector machine is a type of monitoring system that is used to classify or estimate the data fitting function, to create the least error in data grouping or fitting function.

Table 3. Existing models for compressive strength.

Article	Model	Description
Wu[39]	$f_{cc}^{'} = f_c^{'}\left(0.75 + 2.7\left(\frac{f_l}{f_c^{'}}\right)^{0.9}\right)$	$f_l = \frac{2f_{frp}t_j}{D}$
Pham[6]	$f_{cc}^{'} = 0.7f_c^{'} + 1.8f_l + 5.7\frac{t}{D} + 13$	$f_l = \frac{2f_{frp}t_j}{D}$
Ozbakkaloglu[10]	$f_{cc}^{'} = \left(1 + 0.0058\frac{k_1}{f_c^{'}}\right)f_c^{'} + k_1(f_{l,a} - f_{lo})$	$f_{lo} = k_1\left(0.43 + 0.009\frac{k_1}{f_c^{'}}\right)\varepsilon_{co}$
		$k_1 = \frac{2E_{frp}t_j}{D} \geq f_c^{'1.65}$
		$f_{l,a} = \frac{2E_{frp}\varepsilon_{h,rup}t_j}{D}$
Fahmy[40]	$f_{cc}^{'} = f_c^{'} + k_1 f_l$	$f_l = \frac{2f_{frp}t_j}{D}$
		$\begin{cases} k_1 = 4.5f_{l,a}^{-0.3} f_c^{'} \leq 40\,\text{MPa} \\ k_1 = 3.75f_{l,a}^{-0.3} f_c^{'} > 40\,\text{MPa} \end{cases}$
Teng[41]	$\begin{cases} f_{cc}^{'} = f_c^{'}(1 + 3.5(\rho_k - 0.01))\rho_\varepsilon & \rho_k \geq 0.01 \\ f_{cc}^{'} = f_c^{'} & \rho_k < 0.01 \end{cases}$	$\rho_k = \frac{2E_{frp}t_j}{\left(\frac{f_c^{'}}{\varepsilon_{co}}\right)D}, \quad \rho_\varepsilon = \frac{\varepsilon_{h,rup}}{\varepsilon_{co}}$
Youssef[42]	$f_{cc}^{'} = f_c^{'}\left(1 + 2.25\left(\frac{f_l}{f_c^{'}}\right)^{\frac{5}{4}}\right)$	$f_l = \frac{2f_{frp}t_j}{D}$
Kumutha[43]	$f_{cc}^{'} = f_c^{'} + 0.93f_l$	$f_l = \frac{2f_{frp}t_j}{D}$
Guralnick[44]	$f_{cc}^{'} = f_c^{'}\left(0.616 + \frac{f_{l,a}}{f_c^{'}} + 1.57\sqrt{\frac{f_{l,a}}{f_c^{'}} + 0.06}\right)$	$f_{l,a} = \frac{2E_{frp}\varepsilon_{h,rup}t_j}{D}$
Wu-Zhu[45]	$\frac{f_{cc}^{'}}{f_{c0}^{'}} = \frac{f_l}{f_{c0}^{'}} + \sqrt{\left(\frac{16.7}{f_{c0}^{'0.42}} - \frac{f_{c0}^{'0.42}}{16.7}\right)\frac{f_l}{f_{c0}^{'}} + 1}$	$f_l = \frac{2f_{frp}t_j}{D}$
Lam[7]	$f_{cc}^{'} = f_c^{'}\left(1 + 3.3\frac{f_{l,a}}{f_c^{'}}\right)$	$f_{l,a} = \frac{2E_{frp}\varepsilon_{h,rup}t_j}{D}$
Moodi[22]	$f_{cc}^{'} = f_c^{'} + \alpha f_{l,a}$	$\alpha = \begin{cases} \alpha_1 & f_c^{'} \leq 30\,\text{MPa} \\ \alpha_2 & f_c^{'} > 30\,\text{MPa} \end{cases}$
		$\rho_k = \frac{E_{frp}}{f_c^{'}} \quad \rho_\varepsilon = \frac{\varepsilon_{frp}}{\varepsilon_{co}}$
		$k_\varepsilon = f(\rho_k) = \beta_3 + \gamma_3\rho_k^{\lambda_3} + \delta_3\rho_\varepsilon^{\varphi_3} + \theta_3\rho_\varepsilon^{\eta_3}\rho_k^{\zeta_3}$

Note 1. $\beta_3, \gamma_3, \lambda_3, \theta_3, \delta_3, \Phi_3, \eta_3, \zeta_3$ are the optimal values obtained from the genetic optimization algorithm, $\varepsilon_{h,rup}$ is actual rupture strain, ε_0 is unconfined concrete strain.

The purpose of this system is to detect the function $f(x)$ for training model x, so that it has the highest margin of training values y and the least error occurs in the test data.[53] The equation of the function is expressed as follows[54]

$$\boldsymbol{f}(\boldsymbol{x}) = \boldsymbol{W}^T\boldsymbol{X} + \boldsymbol{b} \tag{5}$$

b is the bias component and W is the weight vector x. Given that the optimal value should be the maximum distance from the backup vectors. Therefore, it can be said that[54]

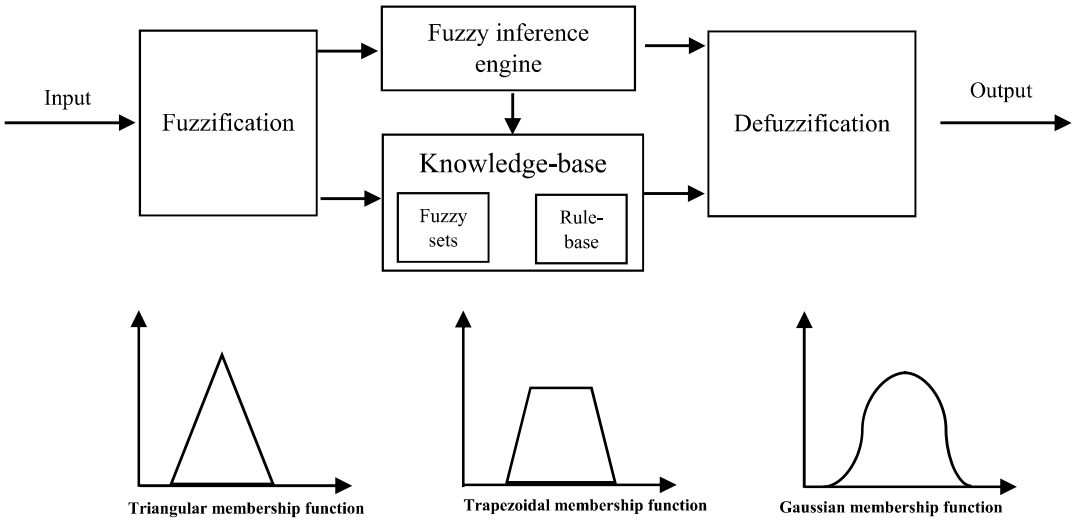

Figure 2. Fuzzy system structure.[48]

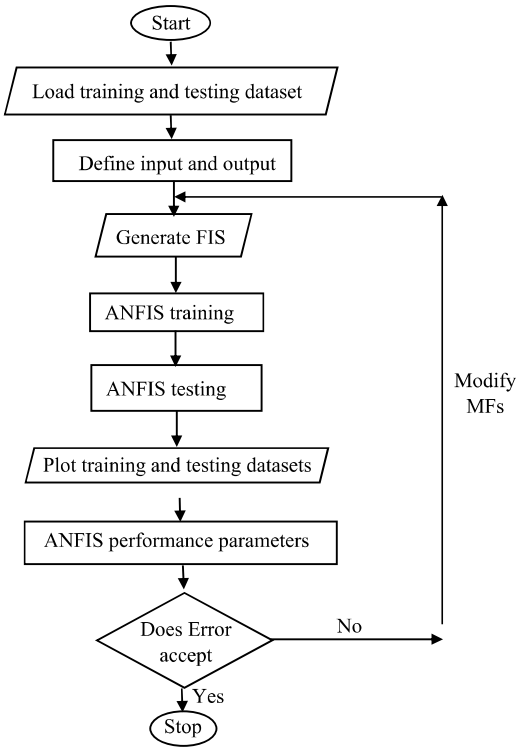

Figure 3. Flowchart of ANFIS process.[51]

$$\textbf{Minimize } \frac{1}{2}\|\mathbf{W}\|^2$$

$$\boldsymbol{S.t.} \begin{cases} \boldsymbol{Y_i} - \boldsymbol{W^T X_i} - b \le \varepsilon \\ \boldsymbol{W^T X_i} + b - \boldsymbol{Y_i} \le \varepsilon \end{cases} \quad (6)$$

Assuming that the data have the violation value of $\xi\hat{}+$ and $\xi\hat{}-$ from their class area, Equation (7) can be rewritten as follows

$$\textbf{Minimize } \frac{1}{2}\|\mathbf{W}\|^2 + \mathbf{C}\sum_{\mathbf{i=1}}^{\mathbf{l}}\left(\xi_{\mathbf{i}}^{+} + \xi_{\mathbf{i}}^{-}\right)$$

$$\boldsymbol{S.t.} \begin{cases} \boldsymbol{Y_i} - \boldsymbol{W^T X_i} - b \le \varepsilon + \xi_i^- \\ \boldsymbol{W^T X_i} + b - \boldsymbol{Y_i} \le \varepsilon + \xi_i^+ \\ \xi_i^-, \xi_i^+ \ge 0 \end{cases} \quad (7)$$

Parameter C in this equation actually acts as a penalty function for data that exceeds the ε threshold. When the data are not linearly separable, the nonlinear space can be mapped to a linear space using the kernel in the above page equation (assuming the data space is multidimensional).[55] The equation is thus expressed as follows

$$\boldsymbol{W^T X} + \boldsymbol{b} = 0 \;\rightarrow\; \boldsymbol{W^T}\phi(\boldsymbol{X}) + \boldsymbol{b} = 0 \quad (8)$$

ϕ is called the kernel function and is responsible for mapping from nonlinear space to linear space. It can also be expressed in general form *K (xi, xj)*. The Gaussian kernel function is defined as follows,[54] which has a high computational efficiency and special performance

$$\boldsymbol{K}(\boldsymbol{X_i}, \boldsymbol{X_j}) = \exp\left(-\gamma \left\|\boldsymbol{X_i} - \boldsymbol{X_j}\right\|^2\right)$$

where the parameter γ represents the spatial distribution and is one of the parameters of the kernel function. Figure 6 shows a flowchart and schematic of the SVR method.

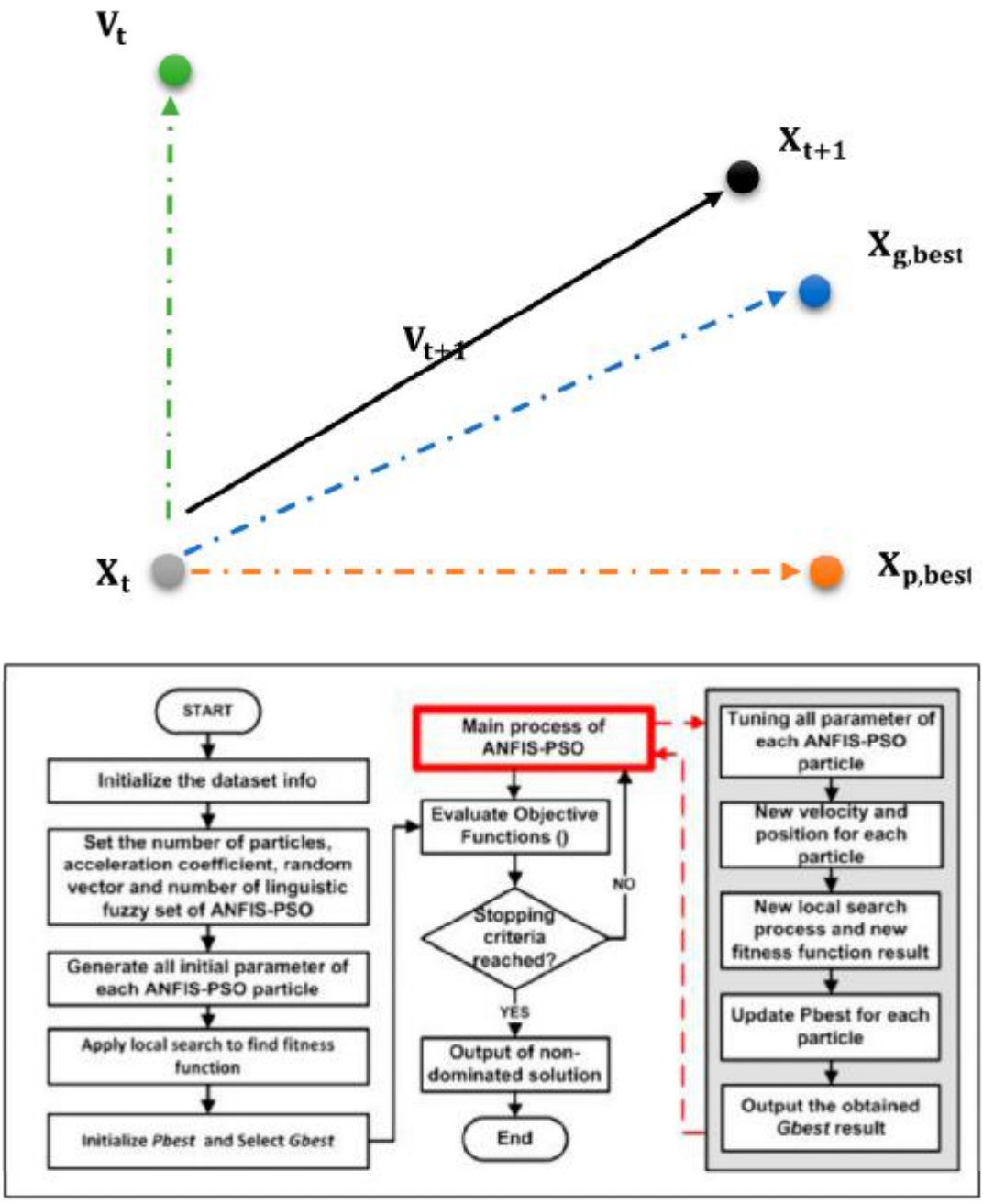

Figure 4. Flowchart of ANFIS-PSO process and the search mechanism of the PSO.[50]

Multilayer perceptron neural network

Multilayer perceptron neural network (MLP) is one of the most widely used types of neural networks in artificial intelligence.[56] The role of the hidden layer is to process and make connections between input and output, which is very important and can be divided into several sublayers.[57]

There are several neurons in each layer of the neural network. The overall behavior of the network depends on the outcome of the behavior of the neurons. Input data is transferred to hidden layers along with weighting to another layer. This is done by transfer functions.[58] These functions are defined as follows

$$\textbf{\textit{Logsig}} \;: f(x) = \frac{1}{1 + e^{x}} \tag{9}$$

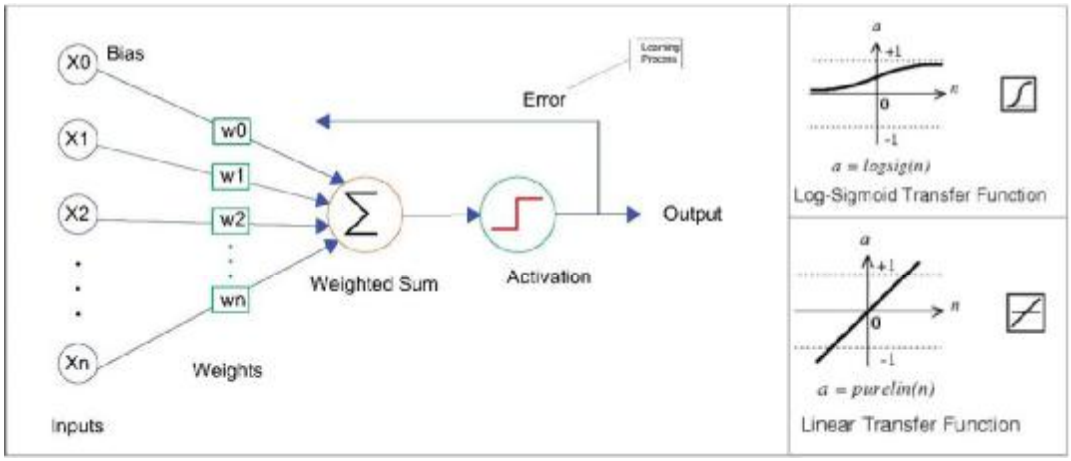

Figure 5. Schematic of a neural network and Transfer functions.[47]

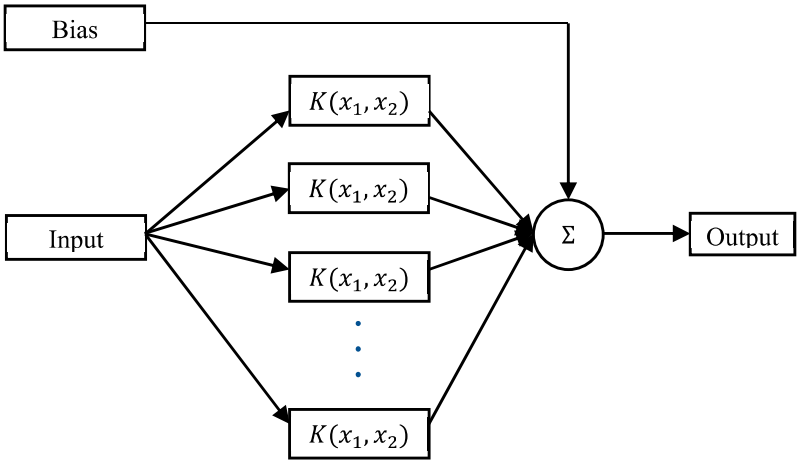

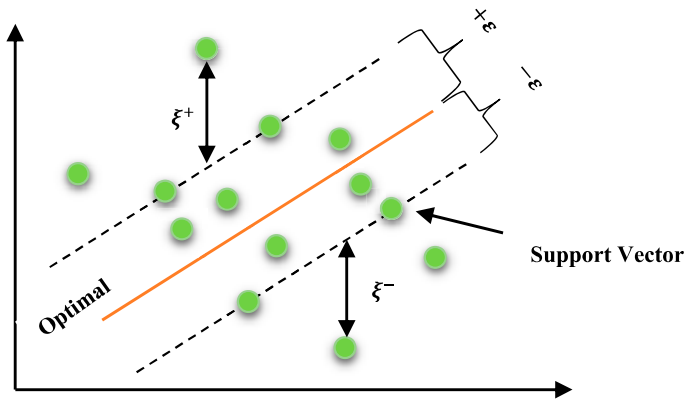

Figure 6. Flowchart and schematic of a typical support vector regression.

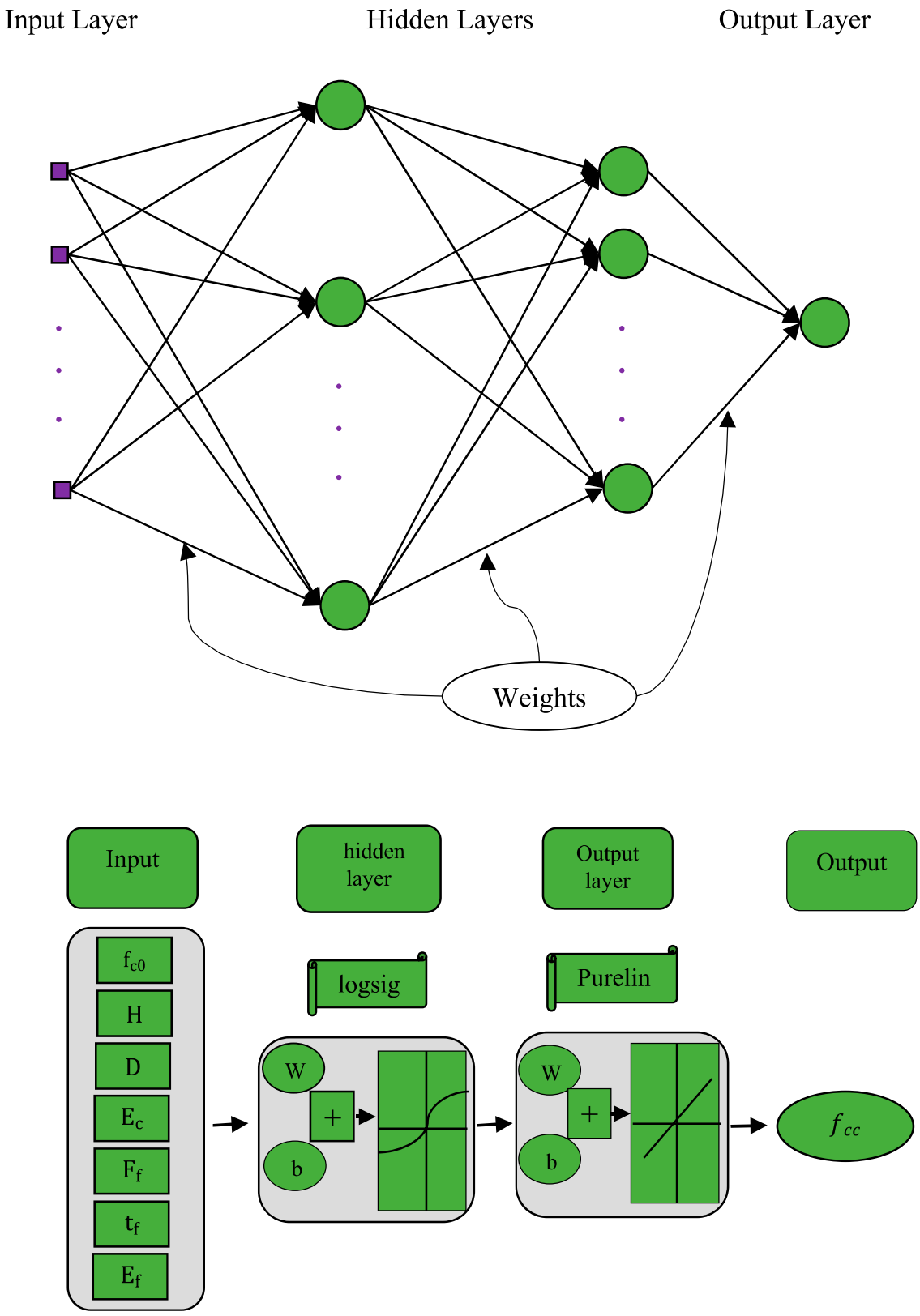

Figure 7. Basic schematic and proposed MLP network for prediction compressive strength.

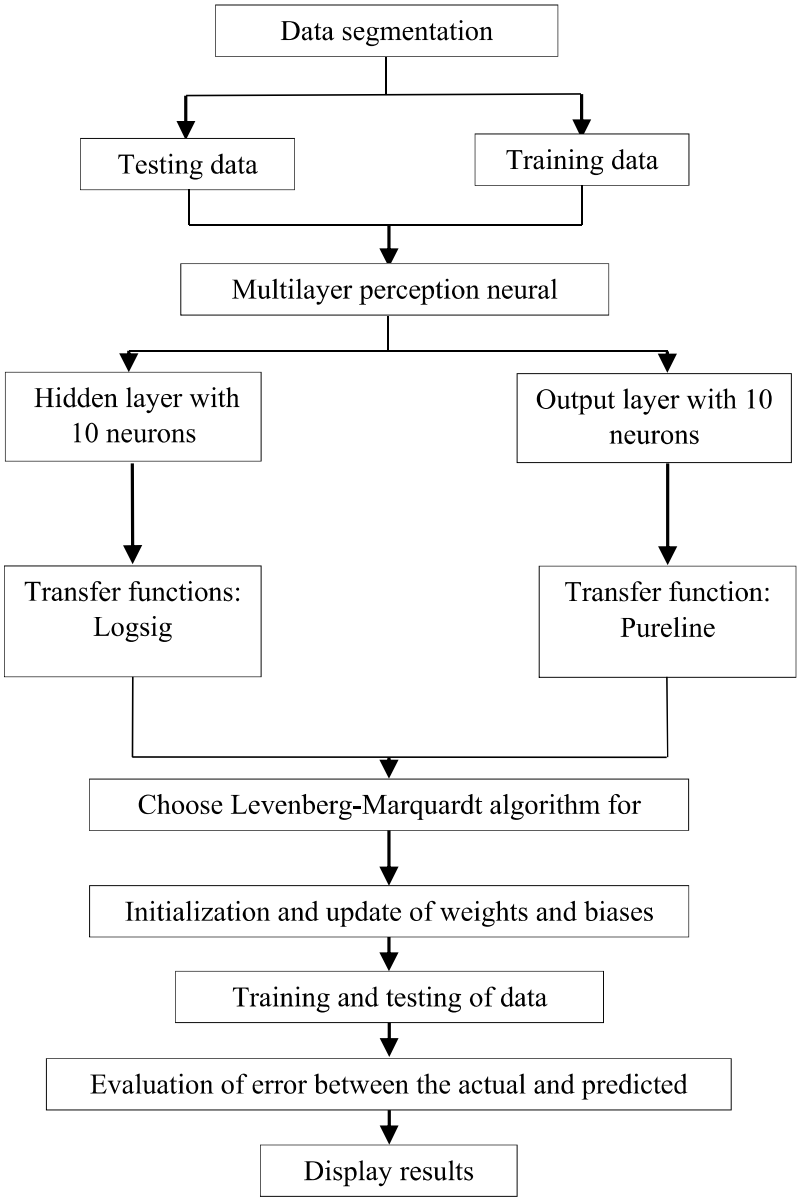

Figure 8. Flowchart of multilayer perceptron neural network with Levenberg–Marquardt algorithm for training.

$$\textit{Pureline} : f(x) = x \tag{10}$$

The training of a Neural network depends on the number of latent and output neurons, and too much or too little of this parameter can lead to network error and wrong training. Also, to ensure the predicted relationship and find the best answer between inputs and outputs, the data should be divided into two categories: training and testing.[58,59] The structure and flowchart of this network are shown in Figure 7 and 8.

Kriging interpolation method

The original idea of this method was developed by Danie G. Krige. This method quickly became a common method as a low-cost simulation method.[60] The kriging estimation method deals with data interpolation based on spatial variance, which is known as a function of distance this model also has enough flexibility to represent nonlinear functions. The kriging method is widely used in reliability assessment and failure probability issues.[61,62] Considering the response function of $G(x)$, the basic kriging model is created in the form of equation (12). $G(x)$ consists of two parts; In this

equation, the first part, $F(x.\beta)$ and the second part, $Z(x)$, are regression models and random processes, respectively.[63,64]

$$\boldsymbol{G}(\boldsymbol{x}) = \boldsymbol{F}(\boldsymbol{x}.\boldsymbol{\beta}) + \boldsymbol{Z}(\boldsymbol{x}) + \boldsymbol{f}(\boldsymbol{x})^{\boldsymbol{T}}\boldsymbol{\beta} + \boldsymbol{Z}(\boldsymbol{x}) \quad (11)$$

where $[f_1(x).f_1(x)\ldots f_m(x)]^T$ and $\beta^T = [\beta_1.\beta_1\ldots\beta_m]^T$ are the basis functions and the corresponding regression coefficient. $F(\boldsymbol{x}.\boldsymbol{\beta}) = F(x.\boldsymbol{\beta}) + Z(\boldsymbol{x})$ is a Gaussian function with a mean value of zero Covariance is presented as equation (12)

$$\boldsymbol{Cov}(\boldsymbol{p},\boldsymbol{r}) = \sigma^2\boldsymbol{R}(\theta.\boldsymbol{p}.\boldsymbol{r}) \quad (12)$$

where $\sigma 2$ and $R\ (\theta.p.r)$ are selected, respectively, by variance and Gaussian correlation function between the points p and r by parameter θ.[64–69]

Method setting parameters

This *Method setting parameters* of the study describes the setting parameters of the estimation methods used. Proper and optimal adjustment of neural network parameters makes the network perform at its best. In an MLP network, the number of layers, the number of neurons in each layer and the transmission functions of each layer are adjustable parameters. Also, the back-propagation error technique has been used in this network. In the SVR network, parameters such as the amount of permissible violation of class privacy, penalty coefficient, kernel function type, and kernel function parameters play the most important roles in achieving the optimal answer. In fuzzy network, fuzzy clustering algorithm (FCM) is used, the function of which is introduced in MATLAB software as genfis3. The setting of the fuzzy method includes the number of clusters, the type of membership functions of inputs and outputs, the number of iterations, and the alpha, which is the parameter for determining the interval of variables in the particle swarm algorithm. The details of the setting parameters mentioned are shown in the Table 4.

Discussion and conclusion

Evaluation of the performance of the proposed estimation methods for predicting compressive strength

Performance of proposed learning machines for estimating the compressive strength of FRP-confined cylindrical

Table 4. Details of the parameters of the methods used.

MLP	**Input activation functions**	**Output activation functions**	**Training algorithm**					
	Logsig	Pureline	Levenberg-Marquardt					
SVR	**Penalty coefficient**	**Violation rate**	**Kernel Function**					
	12750	2.85	Levenberg-Marquardt					
PSO- FIS parameters	**Basic FIS parameters**	**N.O.Iteration**	**Membership Function Type**		**N.O.Cluster**			
			Output	**Input**				
		150	linear	gussmf	15			
	PSO parameters	**N.O. population**		**N.O.Iteration**	**Alpha**			
		70		200	0.8			
ANFIS parameters		**train_StepSizeIncrease**	**train_StepSizeDecrease**	**N.O.Epoch**	**N.O.Iteration**	**Membership Function Type**		**N.O.Cluster**
						Output	**Input**	
		1.15	0.95	250	150	linear	gussmf	20
Kriging		**correlation functions**		**regression polynomial**		**Threshold for equal**		
		Exponential		1 degree		1e-14		

Table 5. Statistical indicators related to the proposed models for predicting ultimate compressive strength.

	Type of network	Mean	Std	MSE	RMSE	IAE	e_{Total}	R
Train data	MLP	0.001	0.133	128.433	11.333	0.138	9.080	0.971
	SVR	−0.159	0.046	15.456	3.931	0.051	3.309	0.996
	ANFIS-PSO	−0.123	0.198	308.170	17.555	0.202	13.222	0.930
	ANFIS	−0.019	0.123	117.587	10.844	0.126	8.259	0.973
	Kriging	0.257	0.041	17.115	4.137	0.026	1.702	0.996
Test data	MLP	−0.334	0.188	249.590	15.798	0.114	11.921	0.957
	SVR	−1.423	0.271	465.128	21.567	0.132	13.614	0.920
	ANFIS-PSO	−0.754	0.225	329.765	18.159	0.132	13.615	0.944
	ANFIS	0.277	0.308	379.163	19.472	0.125	12.982	0.936
	Kriging	−1.298	0.162	194.466	13.945	0.086	8.871	0.967
All data	MLP	−0.100	0.152	164.803	12.838	0.311	9.953	0.966
	SVR	−0.538	0.154	150.442	12.265	0.203	6.481	0.969
	ANFIS-PSO	−0.312	0.207	314.652	17.738	0.419	13.343	0.935
	ANFIS	0.070	0.198	196.109	14.004	0.305	9.713	0.960
	Kriging	**−0.210**	**0.095**	**70.354**	**8.388**	**0.123**	**3.909**	**0.985**

Table 6. Statistical indicators related to existing models for predicting compressive strength.

	Model	Mean	*Std*	*MSE*	*RMSE*	*IAE*	e_{Total}	*R*
All data	Lam	−1.596	0.233	507.139	22.520	0.669	16.555	0.915
	Ozbakkaloglu	1.467	0.229	530.909	23.041	0.656	16.219	0.888
	Wu	−6.211	0.267	777.237	27.879	0.889	21.992	0.885
	Pham	7.084	0.211	454.854	21.327	0.624	15.441	0.917
	Wu-Zho	−1.569	0.216	381.938	19.543	0.583	14.432	0.923
	Fahmy	8.719	0.210	570.679	23.889	0.727	17.986	0.895
	Teng et al.	6.238	0.232	473.155	21.752	0.656	16.236	0.917
	Youssef	1.508	0.305	700.108	26.460	0.675	16.691	0.883
	Kumoto	21.262	0.287	968.091	31.114	0.997	24.652	0.892
	Guralnick	−9.545	0.256	646.939	25.435	0.780	19.290	0.922
	Moodi	−6.64	1.137	6621.860	81.375	1.923	61.247	0.927

specimens has been evaluated using commonly used indicators such as mean error, standard deviation (STD), mean square error (MSE), root mean square error (RMSE), absolute error (IAE) and e_{Total} error, the relationships of which can be seen in Equations (14)–(19), respectively.

$$Mean = \frac{1}{n}\sum_{1}^{n}(exp_i - pred_i) \tag{13}$$

$$STD = \sqrt{\frac{1}{n-1}\sum_{1}^{n}\left(\frac{exp_i - pred_i}{exp_i}\right)^2} \tag{14}$$

$$MSE = \frac{1}{n}\sum_{1}^{n}(exp_i - pred_i)^2 \tag{15}$$

$$RMSE = \sqrt{\frac{1}{n}\sum_{1}^{n}(exp_i - pred_i)^2} \tag{16}$$

$$IAE = \sum_{1}^{n}\frac{|exp_i - pred_i|}{\sum_{1}^{n}|exp_i|} \tag{17}$$

$$e_{Total} = 100 \times \frac{\sum_{1}^{n}|exp_i - pred_i|}{\sum_{1}^{n}|exp_i|} \tag{18}$$

In the above equations, n is the number of specimens, and exp_i and $pred_i$ represent the final compressive strength values of the laboratory specimens and the specimens using soft calculations, respectively. These statistical indices for all specimens, specimens used in education (70%), and specimens used in assessment (30%) are calculated separately in each artificial intelligence method and are presented in Table 5.

According to the results in Table 5, in the test samples that were not used to compare the methods during the training, the kriging method has the lowest error with a value of 8.871. The error of this method in determining

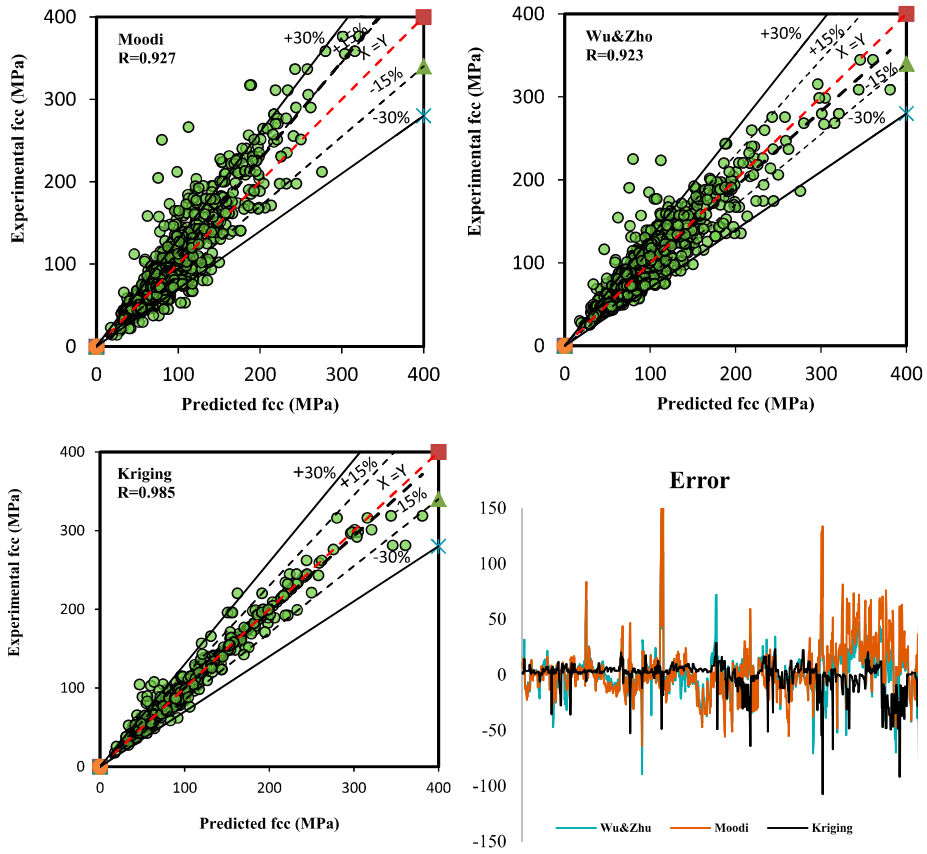

Figure 11. Performance of Moodi, Wu- Zhou, and Kriging models in term of compressive strength.

the compressive strength is 34.3, 53.4, 53.4, and 46.3% less than MLP, SVR, ANFIS-PSO, and ANFIS methods, respectively. When the difference between the error of the training and test samples is checked ($e_{test} - e_{train}$) this difference is greater in the kriging method, and in the ANFIS_PSO method this difference is the smallest. Therefore, ANFIS-PSO and kriging methods can be selected as the best method for estimating compressive strength. Considering all the laboratory data and based on e_{Total}, IAE, RMSE, and MSE indices, the Kriging method has the best performance. Also, by comparing the R parameter, it is observed that the kriging method has the best results in three categories of total data, test data, and training data. According to the above comparison, it can be said that the kriging interpolation method has the best performance in general.

The performance of past analytical models in predicting compressive strength

Based on the results in Table 6, by comparing the statistical indices of MSE, RMSE, IAE, and e_{Total} Mean, Std, the two relationships Moodi and Wu-Zho have better results than other models. Also, the value of coefficient of change R for these two relationships are 0.927 and 0.923, respectively, which have the highest value compared to other models. Figures 9–11 shows a comparison of the results of the mentioned and laboratory models.

Comparison of the performance of artificial intelligence methods with existing models

Based on the results of the previous sections, among the proposed estimation methods, Kriging interpolation method, and from the previous analytical models, Moodi and Wu-Zho relationship presented the best performance. Comparing these three methods with each other, it can be seen that the kriging method has provided better results with a significant difference compared to the Moodi and Wu-Zho models. The results show that the use of the kriging method reduces 64.2, 78.4, and 60.6%, compared to the Moodi relationship and reduces 38, 63.2, and 32.7%, compared to the Wu-Zho relationship in RMSE, IAE, and e_total errors, respectively. Regarding the R

Table 7. Statistical indicators related to best of proposed models versus best existing models for predicting relative compressive strength.

	Type of network	Mean	Std	MSE	RMSE	IAE	e_{Total}	R
Train data	Kriging	0.257	0.041	17.115	4.137	0.026	1.702	0.996
	Moodi	1.591	0.238	365.88	19.128	0.241	15.672	0.825
	Wu-Zho	0.421	0.229	328.183	18.119	0.237	15.393	0.815
Test data	Kriging	−1.298	0.162	194.466	13.945	0.086	8.871	0.967
	Moodi	−25.841	0.279	1522.355	39.017	0.399	22.524	0.934
	Wu-Zho	−6.207	0.183	507.253	22.522	0.234	13.198	0.931
All data	Kriging	−0.210	0.095	70.354	8.388	0.123	3.909	0.985
	Moodi	−6.644	0.251	713.044	26.703	0.755	18.672	0.927
	Wu-Zho	**−1.569**	**0.216**	**381.938**	**19.543**	**0.583**	**14.432**	**0.923**

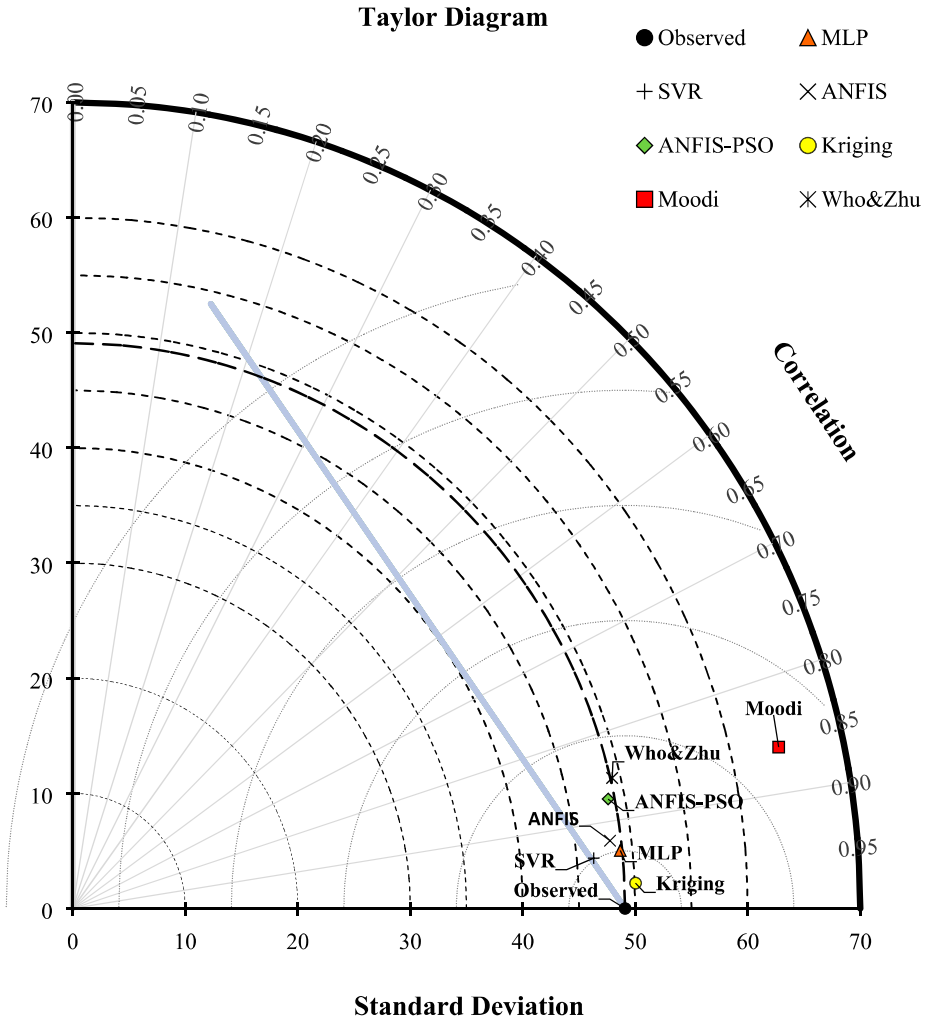

Figure 12. Taylor diagram.

parameter, the kriging interpolation method and the Moodi and Wu-Zho relationship in the total data section obtained the values of 0.985, 0.927, and 0.923, respectively (Table 7).

Taylor diagram

The Taylor diagram compares the correlation values, the mean square root square error, and the standard deviation of the patterns relative to each other and displays it graphically. As shown in Figure 12, the Taylor diagram is shown for the patterns used in this study. In general, artificial intelligence methods have the highest coefficient of R2, the lowest standard deviation, and the amount of RMSE compared to previous models in estimating the compressive strength of concrete. Within the proposed artificial intelligence methods in this field, first kriging and then MLP had the best performance. Other methods also yield good results. It can be said that both provided acceptable results for estimating compressive strength. Also, by comparing the methods of artificial intelligence and the previously presented relationships, according to Taylor diagram, it can be seen that the previous relationships had significant errors compared to the methods presented in this study and gave poorer results than the methods of artificial intelligence.

Conclusion

In this study, a comprehensive database of specimens of FRP-confined concrete cylinders, from previous studies. Aiming to find a complete method with a minimal difference to estimate the compressive strength of FRP-confined concrete, machine learning methods such as (MLPs), (SVR), ANFIS, and their combination with PSO algorithm as well as Kriging interpolation method have been used.

Also, to predict the compressive strength, in addition to the methods proposed in this study, to compare with other existing experimental models, the relationships of previous researchers were collected. This collection contains 1066 specimens. The results of this study can be categorized as follows:

1. Regarding the estimation of the final compressive strength, among these methods, the kriging interpolation method had the lowest error value and showed the highest R coefficient with a value of 0.985. The SVR and MLP networks are in second and third place with R coefficients of 0.969 and 0.966, respectively.
2. Among the experimental models in the previous studies, the Moodi and Wu-Zhu relationships had the best results among the other experimental models with R coefficients of 0.927 and 0.923.
3. By comparing experimental methods and artificial intelligence methods, it was observed that artificial intelligence methods were able to reduce the errors of MSE, RMSE, IAE ,and eTotal errors by 90.1, 68.5, 83.7, and 79%, respectively, and estimate the ultimate compressive strength more accurately than previous relationships.
4. Among the two artificial neural network methods used in this study, the MLP method performed better than the SVR method, so that the total error rate in the MLP method is 12.4% lower than the SVR method.
5. Among the fuzzy logic methods, the difference between the error of the training and test specimens is 0.395 for combining the neural fuzzy system with the particle swarm algorithm and 4.723 for the ANFIS method, which It can be said that the combination of fuzzy neural system with particle swarm algorithm showed better performance in estimating the compressive strength of concrete.

Declaration of Conflicting Interests

The authors declared no potential conflicts of interest with respect to the research, authorship, and/or publication of this article.

Funding

The authors received no financial support for the research, authorship, and/or publication of this article.

ORCID iDs

Seyed Roohollah Mousavi https://orcid.org/0000-0002-8936-9378
Yaser Moodi https://orcid.org/0000-0002-3763-1629

References

1. Teng L, Chen JG, Smith JF, et al. *FRP Strengthened RC Structures*. New York, NY: John Wiley Sons, 2001.
2. Fardis MN, Khalili HH and Marshall AL. FRP-encased concrete as a structural material. *Mag Concr Res* 1982; 34(No. 12112): 191–202.
3. Rousakis T. *"Experimental Investigation of Concrete Cylinders Confined by Carbon FRP Sheet Under Monotonic and Cyclic Axial Compressive Load,"* Res. The Report. Gotenborg, Sweden: Chalmers Univ Thecknology, 2001.
4. Nanni A and Bradford NM. FRP jacketed concrete uniaxial compression. *Constr Build Mater* 1995; 9(No. 2): 115–124.
5. Mander JB, Priestley MJN, et al. Theoretical stress-strain model for confined concrete. *J Struct Eng* 1988 114: 1804–1826.
6. Pham TM and Hadi MNS. Confinement model for FRP confined normal- and high-strength concrete circular columns. *Constr Build Mater* 2014; 69: 83–90.
7. Lam L and Teng JG. Design-oriented stress-strain model for FRP-confined concrete. *Constr Build Mater* 2003; 17: 471–489.

8. Rousakis V, You T, De Lorenzis C, et al. Concrete cylinder confined by carbon FRP sheet subjected to monotonic and cyclic axial compressive loads. In: Proceding 6th International Symposium Fiber Reinforced Polymer Reinforcement For Concrete Structures Singapore, July 2003, 1–10.
9. Sadeghian P and Fam A. Improved design-oriented confinement models for FRP-wrapped concrete cylinders based on statistical analyses. *Eng Struct* 2015; 87: 162–182.
10. Ozbakkaloglu T and Lim JC. Axial compressive behavior of FRP-confined concrete: experimental test database and a new design-oriented model. *Compos Part B: Eng* 2013; 55. 607–634.
11. Keshtegar B, Ozbakkaloglu T and Gholampour A. Modeling the behavior of FRP-confined concrete using dynamic harmony search algorithm. *Eng Comput* 2017; 33: 415–430, DOI: 10.1007/s00366-016-0481-y
12. Keshtegar B, Sadeghian P, Gholampour A, et al. Nonlinear modeling of ultimate strength and strain of FRP-confined concrete using chaos control method. *Compos Struct* 2017; 163: 423–431.
13. Keshtegar B, Gholampour A, Thai D-K, et al. Hybrid regression and machine learning model for predicting ultimate condition of FRP-confined concrete. *Compos Struct* 2021; 262: 113644. DOI: 10.1016/j.compstruct.2021.113644
14. Keshtegar ZM, Bagheri B, Yaseen M, et al. Shear strength of steel fiber-unconfined reinforced concrete beam simulation: application of novel intelligent model. *Compos Struct* 2019; 212: 230–242.
15. Keshtegar R, Nehdi B, Trung ML, et al. Predicting load capacity of shear walls using SVR–RSM model. *Appl Soft Comput* 2021; 112: 107739.
16. Keshtegar B and Yaseen ZM. Reinforcing bar development length modeling using integrative support vector regression model with response surface method: New approach. *ISA transactions*. 2021 Oct 20.
17. El Amine Ben Seghier M, Keshtegar B, Tee BF, et al. Prediction of maximum pitting corrosion depth in oil and gas pipelines. *Eng Fail Analysisþ* 2020; 112: 104505.
18. El Amine Ben Seghier M, Keshtegar B, Amar MN, et al. Simulation of the ultimate conditions of fibre-reinforced polymer confined concrete using hybrid intelligence models. *Eng Fail Anal* 2021; 128: 105605.
19. El Amine Ben Seghier M, Keshtegar B, Taleb-Berrouane M, et al. Advanced intelligence frameworks for predicting maximum pitting corrosion depth in oil and gas pipelines. *Process Saf Environ Prot* 2020; 147: 818–833.
20. Pham TM and Hadi MNS. Predicting Stress and Strain of FRP-Confined Square/Rectangular Columns Using Artificial Neural Networks. J Compos Constr 2014; 18(6): 040140191–040140199. DOI: 10.1061/(ASCE)CC.1943-5614.0000477
21. Sobhani T, Najimi J, Parhizkar M, et al. Prediction of the compressive strength of no-slump concrete: a comparative study of regression, neural network and ANFIS models. *Constr Build Mater* 2010; 24: 709–718.
22. Moodi Y, Mousavi SR and Sohrabi MR. New models for estimating compressive strength of concrete confined with FRP sheets in circular sections. *J Reinf Plast Compos* 2019; 38(21–22): 1014–1028.
23. Kamgar R, Naderpour H, Komeleh HE, et al. A proposed soft computing model for ultimate strength estimation of FRP-confined concrete cylinders. *Appl Sci* 2020; 10(5): 1769. DOI: 10.3390/app10051769
24. Cevik A and Cabalar AF. A genetic-programming-based formulation for the strength enhancement of fiber-reinforced-polymer-confined concrete cylinders. *J Appl Poly Sci* 2008: 110(5): 3087–3095.
25. Cevik A and Guzelbey IH. Neural network modeling of strength enhancement for CFRP confined concrete cylinders. *Building Environ* 2008; 43: 751–763. DOI: 10.1016/j.buildenv.2007.01.036
26. Gandomi AH, Alavi AH and Sahab MG. New formulation for compressive strength of CFRP confined concrete cylinders using linear genetic programming. *Mater Struct* 2010; 43: 963–983. DOI: 10.1617/s11527-009-9559-y
27. Naderpour H, Kheyroddin A and Amiri GG. Prediction of FRP-confined compressive strength of concrete using artificial neural networks. *Compos Struct* 2010; 92(12): 2817–2829. DOI: 10.1016/j.compstruct.2010.04.008
28. Cevik A, Göğüş MT, Güzelbey İH, et al. Soft computing based formulation for strength enhancement of CFRP confined concrete cylinders. *Adv Eng Softw* 2010; 41: 527–536. DOI: 10.1016/j.advengsoft.2009.10.015
29. Cevik A. Modeling strength enhancement of FRP confined concrete cylinders using soft computing. *Expert Syst Appl* 2011; 38(5): 5662–5673. DOI: 10.1016/j.eswa.2010.10.069
30. Elsanadedy HM, Al-Salloum YA, Abbas H, et al. Prediction of strength parameters of FRP-confined concrete. *Compos Part B: Eng* 2012; 43(2): 228–239. DOI: 10.1016/j.compositesb.2011.08.043
31. Jalal M and Ramezanianpour AA. Strength enhancement modeling of concrete cylinders confined with CFRP composites using artificial neural networks. *Compos Part B: Eng* 2012; 43(8): 2990–3000. DOI: 10.1016/j.compositesb.2012.05.044
32. Jalal M, Ramezanianpour AA, Pouladkhan AR, et al. Application of genetic programming (GP) and ANFIS for strength enhancement modeling of CFRP-retro fitted concrete cylinders. *Neural Comput Applic* 2013; 23: 455–470. DOI: 10.1007/s00521-012-0941-2
33. Lim JC, Karakus M and Ozbakkaloglu T. Evaluation of ultimate conditions of FRP-confined concrete columns using genetic programming. *Comput Struct* 2016; 162: 28–37. DOI: 10.1016/j.compstruc.2015.09.005
34. Mansouri I, Ozbakkaloglu T, Kisi O, et al. Predicting behavior of FRP-confined concrete using neuro fuzzy, neural network, multivariate adaptive regression splines and M5 model tree techniques. *Mater Struct* 2016; 49: 4319–4334. DOI: 10.1617/s11527-015-0790-4
35. Mozumder RA, Roy B, Laskar AI, et al. Support vector regression approach to predict the strength of FRP confined concrete. *Arab J Sci Eng* 2016; 42: 1129–1146. DOI: 10.1007/s13369-016-2340-y
36. Cascardi A, Micelli F and Aiello MA. An artificial neural networks model for the prediction of the compressive strength of FRP-confined concrete circular columns. *Eng*

Struct 2017; 140: 199–208. DOI: 10.1016/j.engstruct.2017.02.047

37. Mansouri I, Kisi O, Sadeghian P, et al. Prediction of ultimate strain and strength of FRP-confined concrete cylinders using soft computing methods. *Appl Sci* 2017; 7: 751. DOI: 10.3390/app7080751
38. Ahmad A, Plevris V and Khan Q-Z. Prediction of properties of FRP-confined concrete cylinders based on artificial neural networks. *Crystal* 2020; 10: 811.
39. Wu Y and Wei YF. General stress-strain model for steel- and FRP-confined concrete. *J Compos Constr* 2015; 19: 14.
40. Fahmy Z and Wu MFM. Evaluating and proposing models of circular concrete columns confined with different FRP composites. *Compos Part B* 2010; 41: 199–213.
41. Teng YZ, Jiang JG, Lam T, et al. Refinement of a design-oriented stress–strain model for FRP-confined concrete. *J Compos Constr* 2009; 13(No. 4): 269–278.
42. Youssef AS, Feng MN, Mosallam MQ, et al. 'Stress–strain model for concrete confined by FRP composites. *Compos Part B Eng* 2007; 38: 614–628.
43. Kumutha MS, Vaidyanathan R, Palanichamy R, et al. Behaviour of reinforced concrete rectangular columns strengthened using GFRP. *Cem Concr Compos* 2007; 29: 609–615.
44. Guralnick L and Gunawan SA. Strengthening of reinforced concrete bridge columns with FRP wrap. *Pract Period Struct Des Constr* 2005; 11: 218–228.
45. Wu Y and Zhou Y-W. Unified strength model based on Hoek-Brown failure criterion for circular and square concrete columns confined by FRP. *J Compos Constr*. 2010; 14. [Online]Available: https://ascelibrary.org
46. Fathi M, Rostami S and Mojtaba MS. Prediction of compressive strength of concrete containing fly ash, microsilica and copper slag using statistical methods, artificial neural network and fuzzy logic. *Sharif Civ Eng J* 2019; 34. [Online]. Available. https://civilica.com/doc/894270
47. Bagherzadeh M, Sina and Akbari, "Estimation of compressive strength of concrete using artificial neural network and neural-adaptive fuzzy inference system," *10th Int. Congr. Civ. Eng. Tabriz*, 1394, [Online]. Available: https://civilica.com/doc/364640. In Persian
48. Jagan JSR, ANFIS: adaptive-network-based fuzzy inference system. *IEEE Trans Syst Man Cybern*. 1993; 23(No.3): 665–685.
49. Gencel O, Brostow W, Beycioğlu A, et al. Estimation of fracture energy of high-strength steel fibre-reinforced concrete using rule-based Mamdani-type fuzzy inference system. *Sci Eng Compos Mater* 2012; 19(4): 373–380.
50. Robati FN and Iranmanesh S. Inflation rate modeling: adaptive neuro-fuzzy inference system approach and particle swarm optimization algorithm (ANFIS-PSO). *MethodX* 2020; 7: 101062.
51. Abdel-Aleem1 A, El-Sharief1 MA, El-Sebaie1 Mohamed G, et al. Implementation of fuzzy and adaptive neuro-fuzzy inference systems in optimization of production inventory problem. *Appl Math Inf Sci* 2017; 11(No. 1): 289–298.
52. Shaban M, Yang J, Elbaz K, et al. Fuzzy-metaheuristic ensembles for predicting the compressive strength of brick aggregate concrete. *Resour Conserv Recycl* 2021; 169–105443.
53. Yuvaraj PSP, Ramachandra Murthy A, Iyer NR, et al. Support vector regression based models to predict fracture characteristics of high strength and ultra high strength concrete beams. *Eng Fract Mech* 2013; 98: 29–43.
54. Sun GMJ, Zhang J, Gu Y, et al. Prediction of permeability and unconfined compressive strength of pervious concrete using evolved support vector regression. *Constr Build Mater* 2019; 207: 440–449.
55. Vapnik VN. An overview of statistical learning theory. *IEEE Trans Neural Networks* 1999; 10: 988–999.
56. Mokhtari S and Mooney MA. Predicting EPBM advance rate performance using support vector regression modeling. *Tunn Undergr Sp Technol* 2020; 104: 103520.
57. Ouaer H, Hosseini AH, Nait Amar M, et al. Rigorous connectionist models to predict carbon dioxide solubility in various ionic liquids. *Appl Sci* 2020; 10: 304.
58. Abdi-Khanghah M, Bemani A, Naserzadeh Z, et al. Prediction of solubility of N-alkanes in supercritical CO2 using RBF-ANN and MLP-ANN. *J Compos Constr* 2018; 25: 108–119.
59. Ghritlahre HK and Prasad RK. Exergetic performance prediction of solar air heater using MLP, GRNN and RBF models of artificial neural network technique. *J Environ Manage* 2018; 223: 566–575.
60. Jones DR, Schonlau M and Welch WJ. Efficient global optimization of expensive black-box functions. *J Glob Optim* 1998; 13: 455–492.
61. Sacks J, Welch WJ, Mitchell TJ, et al. Design and analysis of computerexperiments. *Stat Sci* 1989; 4: 409–423.
62. Zhou Y, Lu ZZ and Cheng K. A bayesian monte carlo-based method for efficient computation of global sensitivity indices. *Mech Syst Signal Process* 2019; 117(5): 498–516.
63. Matheron G. The intrinsic random functions and their applications. *Adv Appl Probab* 1973; 5(3): 439–468.
64. Flores EI, DiazDelaO FA and Friswell MI. A computational multi-scale approach for the stochastic mechanical response of foam filled honeycomb cores. *Compos Struct* 2012; 94: 1861–1870.
65. Ling C, Lu Z, Sun B, et al. An efficient method combining active learning kriging and monte carlo simulation for profust failure probability. *Fuzzy Sets Syst*s2020; 387: 89–107.
66. Leigang Z, Zhenzhou L and Wang P. Efficient structural reliability analysis method based on advanced Kriging model. *Appl Math Model* 2015; 39: 781–793.
67. Moodi Y, Shahri FS and Mousavi SR. Providing a model for estimating the compressive strength of square and rectangular columns confined with a variety of fibre-reinforced polymer. *J Reinf Plast Compos* 2017; 36(21): 1602–1612. DOI: 10.1177/0731684417720837
68. Ghasemi H, Sohrabi MR and Moodi Y. Proposing models for estimating the compressive strength of HSC and UHSC FRP-confined circular concrete by using whale algorithm. *Iran J Sci Technol Trans Civ Eng* 2021, Online Publication. DOI: 10.1007/s40996-021-00655-2
69. Moodi Y, Sohrabi MR and Mousavi SR. Corrosion effect of the main rebar and stirrups on the bond strength of RC

beams, Structures. *Sciencedirect* 2021; 32: 1444–1454. DOI: 10.1016/j.istruc.2021.03.096
70. Aire D, Gettu C, Casas R, et al. Concrete laterally confined with fibre-reinforced polymers (FRP): experimental study and theoretical model'. *Material Constr* 2010; 60(29): 19–31.
71. Akogbe M, Wu RK and Liang ZM. Size effect of axial compressive strength of cfrp confined concrete cylinders. *Int J Concr Struct Mater* 2011; 5(1): 49–55.
72. Al-Salloum N and Siddiqui Y. Compressive strength prediction model for FRP confined concrete. In: Proceding 9th International Symposium FRP Fiber Reinforced Polymer Reinforcement for Concrete Structures. Sydney, Australia, 2009.
73. Benzaid NE, Mesbah R and Chikh H. FRP-confined concrete cylinders: axial compression experiments and strength model. *J Reinf Plast Compos* 2010; 29(16): 2469–2488.
74. Berthet JF, Ferrier E and Patrice H. Compressive behavior of concrete externally confined by composite jackets. Part A: experimental study. *Constr Build Mater* 2005; 19(3): 223–232.
75. Bisby LA, Take WA and Caspary A. Quantifying strain variation FRP confined using digital image correlation proof of concept and initial result. *Asia-Pacific Conf FRP Struct* 2007: 599–604.
76. Bisby K, Chen LA, Li JF, et al. Strengthening fire-damaged concrete by confinement with fibre-reinforced polymer wraps. *Eng Struct* 2011; 33(12): 3381–3391.
77. Carnpione N, Miraglia G and Scibilia N. Compressive behavior of RC members strengthened with carbon fiber reinforced plastic layers. *Trans Built Environ* 2001; 57: 397–406.
78. Carey KA and Harries SA. Axial behavior and modeling of confined small-, medium-, and large-scale circular sections with carbon fiber-reinforced polymer jackets. *ACI Struct J* 2005; 102(4): 596–604.
79. Cui C and Sheikh SA. Experimental study of normal-and high-strength concrete confined with fiber-reinforced polymers. *J Compos Constr* 2010; 14(5): 553–561.
80. Demers K and Neale M. Strengthening of concrete columns with unidirectional composite sheets. *Proc Dev Short Mediu Span Bridg Eng Montr Que*. 1994.
81. Elsanadedy HM, Al-Salloum YA, Alsayed SH and Iqbal RA. Experimental and numerical investigation of size effects in FRP-wrapped concrete columns. *Construction and Building Materials*. 2012 Apr 1; 29: 56–72.
82. Erdil IO, Akyuz BU and Yaman U. Mechanical behavior of CFRP confined low strength concretes subjected to simultaneous heating-cooling cycles and sustained loading. *Mater Struct* 2012; 45: 223–233.
83. Evans T, Kocman J and Kretschmer M. Hybrid FRP Confined Concrete Columns. Adelaide, Australia: School Civil Environ Min Eng Univ, 2008.
84. Green VKR, Bisby MF, Fam LA, et al. FRP confined concrete column: behavior under extreme conditions. *Cem Concr Compos* 2006; 28: 928–993.
85. Harmon KT and Slattery TG. Advanced composite confinement of concrete. In: Proceding Advance Composite Material Bridge Structure. Montereal, Canada, 1992.
86. Harries G and Kharel KA. Behavior and modeling of concrete subject to variable confining pressure. *ACI Mater J* 2002; 99: 180–189.
87. Ilki A, Kumbasar N and Kov V. Strength and deformability of low strength concrete confined by carbon fiber composite sheets. In: Procedings 15th Engineering Mechanics Conference, New York, 2002.
88. Issa CA. The effect of elevated temperatures on CFRP wrapped concrete cylinders. In: Proceeding 8th International Symposium on Fiber Reinforcement Concrete. Structure. Greece, 2008.
89. Karabinis TC and Rousakis AI. Concrete confined by FRP material: a plasticity approach. *ASCE J Eng Struct* 2002; 24(7): 923–932.
90. Karam M and Tabbara GN. Corner effects in CFRP-wrapped square columns. *Mag Concr Res* 2004; 56(8); 461–464.
91. Karantzikis M, Papanicolaou CG, Antonopoulos CP, et al. Experimental investigation of nonconventional confinement for concrete using FRP. ASCE J Compos Constr 2005; 9(6): 480–487.
92. Karbhari Y and Gao VM. Composite jacketed concrete under uniaxial compression—verification of simple design equations. *J Mater Civ Eng* 1997; 9(4): 185–193.
93. Kono T, Inazuni S and Kaku M. Evaluation of confining effects of CFRP sheets on reinforced concrete members. In: Proceeding 2nd International Conference Composite Infrastructures 1998; 1: 343–355.
94. Lam G and Teng L. Ultimate condition of FRP confined concrete. *J Compos Constr* 2004; 8(6): 539–548.
95. Lam Y, Teng L, Cheung JG, et al. FRP-confined concrete under axial cyclic compression. *Cem Concr Compos* 2006; 28(10): 949–958.
96. Lee J, Yi J, Jeong C, et al. Compressive response of concrete confined with steel spirals and FRP composites. *J Compos Mater* 2009; 44(4): 481–504.
97. Lin CI and Liao HJ. An effective peak stress formula for concrete confined with carbon fiber reinforced plastics. *J Civ Eng* 2003; 30: 882–889.
98. Liang R, Wu M, Ueda Z, et al. Experiment and modeling on axial behavior of carbon fiber reinforced polymer confined concrete cylinders with different size. *J Reinfor Plastics Compos* 2012; 31(6): 389–403.
99. Mandal A, Hoskin S and Fam A. Influence of concrete strength on confinement effectiveness of fiber reinforced polymer circular jackets. *Struct J* 2005; 102: 383–392.
100. Matthys K, Taerwe S and Audenaert L. Tests on axially loaded concrete columns confined by fiber reinforced polymer sheets wrapping. In: Procedings 4th International Symposium Fiber Reinforcemet Polymer Reinforcement Concrete Structure, Mainz, Germany, 4 October 1999, 1999: 217–228.
101. Miyauchi S, Nishibayashi K and Inoue S. Estimation of strengthening effects with carbon fiber sheet for concrete column. In: Procedings 3rd Int Symposium Non-metalic Reinforcement Concrete Structure, Sapporo, Japan, 14–16 October 1997, 1997.
102. Modarelli O, Micelli R and Manni F. FRP confinement of hollow concrete cylinders and prisms. In: Proceeding 7th International Symposium Fiber Reinforcement Polymer Reinforcement Concretere Structure, Kansas City, MI, 2005.

103. Owen LM. *Stress-strain Behavior of Concrete Confined by Carbon Fiber Jacketing*. Washington, Seattle: Masters, Univ, 1998.
104. Ongpeng JMC. Retrofitting RC circular columns using CFRP sheet as confinement. Symposium on Infrastructure Development and the Environment 2006, Quezon City, Philippines, 2006.
105. Song WX, Gu X, Li Y, et al. Mechanical behavior of FRP strengthened concrete columns subjected to concentric and eccentric compression loading. *J Compos Constr* 2013; 17(3): 336–346.
106. Shehata LAEM, Carneiro IAV and Shehata L. Strength of short concrete columns confined with CFRP sheet. *Mater Struct* 2002; 35: 50–58.
107. Shehata LAEM, Carneiro IAV and Shehata L. Strength of confined short concrete columns. In: 8th International Symposium Fiber Reinforcement Polymer Reinforcement Concrete Structure Patras. Greece, 2002.
108. Stanton JF and Owen LM. *The influence of concrete strength and confinement type on the response of FRP-confined concrete cylinders*. Special Publication. 2006 Oct 1; 238: 347–362.
109. Tamuzs K, Valdmins V, Tepfer V, et al. Stability analysis of CFRP wrapped concrete columns strengthened with external longitudinal CFRP sheet. *Mech Compos Mater* 2008; 44: 199–208.
110. Theriault S, Neale MKW and ASCEClaude M. Fiber reinforced polymer confined circular concrete columns: investigation of size and slenderness effects. *J Compos Constr* 2004; 8(No. 4): 323–331.
111. Valdmanis RV, De Lorenzis L, Rousakis T, et al. Behavior and capacity of CFRP confined concrete cylinder subjected to monotonic and cyclic axial compressive loads. *Struct Concr* 2007; 8(4): 187–200.
112. Vincent T and Ozbakkaloglu T. Influence of concrete strength and confinement method on axial compressive behavior of FRP confined and ultra high strength concrete. *Compos Part B Eng* 2010; 50: 413–428.
113. Picher P, Rochette F, Com P, et al. Confinement of concrete cylinders with CFRP. In: Proceeding Is International Conference Composite Infrastructure. Tuscon, Arizona, 1996.
114. Pressure Piekarczy J, Piekarczy W and Blazewichz S. Compressive strength of concrete cylinders reinforced with carbon fiber laminate. *Constr Build Mater* 2011; 25:2365–2369.
115. Rochette P and Labossière P. Axial testing of rectangular column models confined with composites. *ASCE J Compos Constr* 2000; 4(3): 129–136.
116. Saenz CP and Pantelides N. Short and medium term durability evaluation of FRP confined circular concrete. *J Compos Constr* 2006; 10(3): 244–253.
117. Santaros JL, Filho D, Beber AC, et al. Concrete columns confined with CFRP sheet. In: Proceeding International Conferene FRP Composite Civil Engineering. Hong Kong 2001.
118. Shahawy BM and Mirmiran A. Tests and modeling of carbon wrapped concrete columns. *Compos Part B Eng* 2000; 31(6): 471–480.
119. Smith ST, Kim SJ and Zhang H. 'Behavior and effectiveness of FRP Wrap in the confinement of large concrete cylinders. *J Compos Constr* 2010; 14(5): 573–582.
120. Wang YF and Wu LM. Effect of corner radius on the performance of CFRP-confined square concrete columns: test. *Eng Struct* 2008; 30(2): 493–505.
121. Xiao H and Wu Y. Compressive behavior concrete confined by carbon fiber composites jackets. *J Mater Civ Eng* 2000; 12(2): 139–146.
122. Wu JJF and Jiang YF. Effective strain of FRP confined circular concrete columns. *Compos Struct* 2013; 95: 479–491.
123. Shao A, Zhu Y and Mirmiran Z. Cyclic modeling of FRP confined concrete with improved ductility. *Cem Concr Compos* 2006; 2(10): 956–968.
124. Silva MAG and Chastre C. Size and relative stiffness effects on compressive failure of concrete columns wrapped with glass FRP. *J Mater Civ Eng* 2006; 18: 334–342.
125. Zhang YW, Ye S and Mai L. Study on polymer composite strengthening systems for concrete columns. *Appl Compos Mater* 2000; 7: 125–138.
126. Ahmad A, Khaloo SH and Irshaid AR. Behavior of concrete spirally confined by fiberglass filaments. *Mag Concr Res* 1991; 43(15): 143–148.
127. Au O and Buyukozturk C. Effect of fiber orientation and ply mix on fiber reinforced polymer-confined concrete. *J Compos Constr* 2005; 9(5): 397–407.
128. Bullo S. Experimental study of the effect the ultimate strain of fiber reinforced plastic jackets on the behavior of confined concrete. In: Procedings International Conference Composite Construction. Cosenza, Italy. 2003.
129. Comert A, Goksu M and Ilki C. Towards a tailored stress-strain behaviour for FRP confined low strength concrete. In: Procedings 9th International Symposium Fiber Reinforcement Polymer Reinforcenment Concrete Structure. Sydney, Australia, 2010.
130. Harries A and Carey KA. Shape and "gap" effects on the behavior of variably confined concrete. *Cem Concr Res* 2003; 33: 881–889.
131. Dai JG, Bai JG and Teng YL. Behavior and modeling of concrete confined with FRP composites of large deformability. *J Compos Constr* 2011; 15: 963–973.
132. Teng SL, Yu JG, Wong T, et al. Hybrid FRP concrete steel tubular columns: concept and behavior. *Constr Build Mater* 2007; 21: 846–854.
133. Ozbakkaloglu T and Akin E. Behavior of FRP-confined normal-and high-strength concrete under cyclic axial compression. *J Compos Constr* 2012; 16(4): 451–463.
134. Suter R and Pinzelli R. Confinement of concrete columns with frp sheet. In: Proceeding 5th Symposium Fiber Reinforcement Plast. Reinforcement Concrete Structure, London, 2001.
135. Wang Y-f and Wu H-L. Size effect of concrete short columns confined with aramid FRP jacket. *ASCE J Compos Constr* 2011; 15: 535–544.
136. Jiang JG and Teng T. Analysis-oriented stress–strain models for FRP–confined concrete. *Eng Struct* 2007; 29: 2968–2986.
137. Mirmiran H, Shahawy A, Samaan M, et al. Effects of column parameters on FRP confined concrete. *J Compos Constr* 1998; 2 175–185.
138. Yan D, Pantelides Z and Reaveley CP. Fiber reinforced polymer jacketed and shape modified compression member: I-experimental behavior. *ACI Struct J* 2006; 6: 885–893.
139. Li M, Maricherla G, Singh D, et al. Effect of fiber orientation on the structural behavior of FRP wrapped concrete cylinder. *J Compos Struct* 2006; 74: 475–483.

140. Watanabe N, Nakamura K, Honda R, et al. Confinement effect of FRP sheet on strength and ductility of concrete cylinders under uniaxial compression. *Proc Third Int Symp* 1997; 1: 233–238.
141. Wong SL, Yu Y.L, Teng T, et al. Behavior of FRP-confined concrete in annular section columns. *Compos Part B Eng* 2008; 39: 451–466.
142. Micelli S, Myers F and Murthy JJ. Effect of environmental cycles on concrete cylinders confined with FRP. In: Proceeding International Conference Composite Construction. Porto, Port, 2001.
143. Hosotani J, Kawashima K and Hoshikuma K. A model for confinement effect for concrete cylinders confined by carbon fiber sheets. In: Workshop on Earthquake Engineering Frontiers in Transportation Facilities. Buffalo, NY, 1997.
144. Mastrapa JC. *Effect of construction bond on confinement with fiber composites*. Orlando, FL. Masters, Univ Cent, 1997.
145. Wu ZS, Lü G and Wu ZT. Strength and ductility of concrete cylinders confined with FRP composites. *Constr Build Mater* 2006; 20: 134–148.
146. Wu YB, Wu G, Lu ZS, et al. Structural performance of concrete confined with hybrid FRP composites. *J Reinf Plast Compos* 2008; 27: 1323–1348.
147. Wu XH., Wang Y, Yu L, et al. Experimental and computational studies on high strength concrete circular columns confined by aramid fiber reinforced polymer sheet. *J Compos Constr* 2009; 13(2): 125–134.
148. Vincent T and Ozbakkaloglu T. Influence of concrete strength and confinement method on axial compressive behavior of FRP confined and ultra high strength concrete. *Compos Part B Eng* 2010; 50: 413–428.
149. Ilki V, Kumbasar A and Kov N. Low strength concrete members externally confined with FRP sheet. *Struct Eng Mech* 2004; 18: 167–194.
150. Lin CT and Chen HJ. Strength of concrete cylinder confined by composite materials. *J Reinf Plast Compos* 2001; 20: 1577–1600.
151. Howie VM and Karbhari I. Effect of materials architecture on strengthening efficiency of composite wraps for deteriorating columns in the north-east. In: 3rd Materials engineering conference, San Diego, CA, 1994.
152. Issa GN and Karam CA. Compressive strength of concrete cylinders with variable widths CFRP wraps. In: Proceeding 4th International Conference Advanced Composite Mater Bridge Structure. Calgry, AL, 2004.
153. Lin CI and Liao HJ. Compressive strength of reinforced concrete column confined by composite material. *J Compos Struct* 2004; 65: 239–250.
154. Miyauchi K, Inoue S, Kuroda T and Kobayashi A. Strengthening effects with carbon fiber sheet for concrete column. *Proc Jpn Concr Inst*. 1999 Mar; 21(3): 1453–1458.
155. Abdollahi M, Bakhshi B and Shekarchi M. Experimental modeling of GFRP confined concrete cylinders subjected to axial loads. In: Procedings 8th International Symposium FRP Reinforcement Concrete Structure. Patras, Greece, 2007.
156. Almusallam T. Behavior of normal and high-strength concrete cylinders confined with E-glass/epoxy composite laminates. *Compos Part B Eng* 2007; 38(5–6): 629–639.
157. Wang Y and Zhang D. Creep-effect on mechanical behavior of concrete confined by FRP under axial compression. *ASCE, J Eng Mech* 2009; 135(11): 1315–1322.
158. Park S, Jo JH and Yoon BW. Experimental investigation on the structural behavior of concrete filled FRP tubes with/without steel Re-bar. *KSCE J Civ Eng* 2011; 15(2): 337–345.
159. Saafi MA, Toutanji HA and Li Z. Behavior of concrete columns confined with fiber reinforced polymer tubes. *ACI Struct J* 1999; 96(5): 500–509.
160. Aire C, Gettu R, Casas JR, et al. Concrete laterally confined with fibre-reinforced polymers (FRP): experimental study and theoretical model. *Mater Constr* 2010; 60: 19–31.
161. Chikh N BR and Gahmous M. Structural performance of high strength concrete columns confined with CFRP sheets. In: Papaer Presented at Procedings World Congress Engineering, London, UK, 2012.
162. Green MF. FRP repair of concrete structures: performance in cold regions. *Int J Mater Prod Technol* 2007; 28(1–2): 160–177.
163. Aire C, Gettu R and Casas JR. Study of the compressive behavior of concrete confined by fiber reinforced composites. In: International Conference on Composites in Constructions, Porto, Portugal, 10 December 2001. The Netherlands: AA Balkema Publ. Lisse, 2001, 239–243.
164. Benzaid R, Chikh NE and Mesbah HA. Study of the compressive behavior of short concrete columns confined by fiber reinforced composite. *Arab J Sci Eng* 2021; 34(1B): 15–26.
165. Mandal S. Axial loading tests on FRP confined concrete of different compressive strengths. In: Proceedings, 4th Advanced Composite Materials Bridges and Structures. Alberta, Canada, 2004.
166. Ozbakkaloglu T and Vincent T. Axial compressive behavior of circular high-strength concrete-filled FRP tubes. *ASCE* 18, 2014.
167. Valdmanis V TR., De Lorenzis L and Rousakis T. Behaviour and capacity of CFRP-confined concrete cylinders subjected to monotonic and cyclic axial compressive load. *Structural Concrete* 8. Published Online, 2007.
168. Xiao Q, Teng JG and Yu T. Behavior and modeling of confined high-strength concrete. *J Compos Constr* 2010; 14(3): 249–259, DOI: 10.1061/(ASCE)CC.1943-5614.0000070
169. Cao Q, Li X and Goa R. Axial compressive performance of CFRP confined self-stressing high-strength concrete cylinders. *KSCE J Civ Eng* 2019; 23(9): 4000–4009.
170. Vincent T and Ozbakkaloglu T. Influence of prestress on axial compressive behavior of high-strength concrete-filled FRP tubes. In: Paper Present Applied Mechnical. Materials, Xiamen, China, 2015. https://doi.org/10.4028/
171. de Oliveira DS, Raiz V and Carrazedo R. Experimental study on normal-strength, high-strength and ultrahigh-strength concrete confined by carbon and glass FRP laminates. *J Compos Constr* 2019; 23(1): 04018072.
172. Adam Ostrowski K. The influence of CFRP sheets on the strength of specimens produced using normal concrete and high-performance concrete assessed using uniaxial compression tests. *Czas Tech* 2017; 7: 41–51.
173. Touhari M and Mitiche-Kettab R. Behaviour of FRP confined concrete cylinders: Experimental investigation and strength model. *Period Polytech Civ Eng* 2016; 60(4): 647–660.
174. Wakjira TG, Alam MS and Ebead U. Plastic hinge length of rectangular RC columns using ensemble machine learning model. *Eng Struct* 2021; 244: 112808. DOI: 10.1016/j.engstruct.2021.112808

Appendix 1

Table A1. The collected experimental specimen details.

Number	References	No. of specimens	Diameter (mm)	Height(mm)	Unconfined concrete strength range (MPa)	Mudul elasticity of FRP	FRP strength	Thickness of FRP	FRP type
1	Aire et al.[70]	6	150	300	42	65–240	3000–3900	0.117–0.894	CFRP, GFRP
2	Akogbe et al.[71]	12	100–300	200–600	21.7–26.5	242	3248	0.167–0.501	CFRP
3	Al-salloum[72]	2	150	300	32.4–36.2	75.1	935	1.2	CFRP
4	Benzaid et al.[73]	6	160	320	25.9–49.5-61.81	238–240	4300–3900	0.13–0,39 62.68–93.2	CFRP
5	Berthet et al.[74]	48	160 70	320 140	25–52 112.6–169.7	74–230 240	2500–3200 3900	0.11–0.99 141.1–296.4	CFRP, GFRP
6	Bisby et al.[75]	3	150	300	34.4	231	4100	0.12	CFRP
7	Bisby et al.[76]	3	100	200	28	231	4100	0.12	CFRP
8	Carnpione et al.[77]	1	100	200	20.1	230	3430	0.165	CFRP
9	Carey and Harries[78]	2	152–254	305–762	33.5–38.9	72.5–251	350–875	1–1.7	CFRP
10	Cui and Sheikh[79]	64	152	305	45.6–48.1 79.9–111.8	22–436 240–377	508.2–3314 3900–4410	0.11–3 105.3–153.3	CFRP,GFRP,HM-CFRP
11	Demers and Neale[80]	8	152	305	32.2–43.7	10.5–25	220–380	1_3	CFRP,GFRP
12	Elsanadedy et al.[81]	6	50–150	100–300	41.1–53.8	77.3	846	1_4	CFRP
13	Erdil et al.[82]	2	150	300	11.1–20.8	230	3430	0.165	CFRP
14	Evans et al.[83]	2	152	305	37.3–46	240–22.4	3800–237	0.234–1	CFRP,HFRP
15	Green et al.[84]	3	152	305	46–54	8.8–22.4	182–237	1_2	CFRP,GFRP
16	Harmon and Slattery[85]	3	51	102	41	235	3500	0.09–0.69	CFRP
17	Harries and Kharel[86]	10	152	305	32.1	4.9–25	75–350	1_15	CFRP,GFRP
18	Iliki et al.[87]	5	150	300	32	230	3430	0.165–0.825	CFRP
19	Issa[88]	3	150	300	23.6–23.9	231	4100	0.12	CFRP
20	Karabinis[89]	16	200	320	35.7–38.5	240	3720	0.117–0.351	CFRP
21	Karam and Tabbra[90]	2	150	300	12.8	231	3650	0.12–0.24	CFRP
22	Karantzikis et al.[91]	1	200	350	12.1	230	3500	0.12	CFRP
23	Karbhari and Gao[92]	3	152	305	38.4	227	3500	0.66–1.32	CFRP
24	Kono et al.[93]	15	100	200	34.3–34.8	235	3820	0.167–0.501	CFRP
25	Lam and Teng[94]	18	152	305	34.3–38.5	22.46–230	450–3420	0.165–2.54	CFRP,GFRP
26	Lam et al.[95]	6	152.5	305	38.9–41.1	250.5	3795	0.165–0.33	CFRP

(continued)

(continued)

Number	References	No. of specimens	Diameter (mm)	Height(mm)	Unconfined concrete strength range (MPa)	Mudul elasticity of FRP	FRP strength	Thickness of FRP	FRP type
27	Lee et al.[96]	5	150	300	36.2	250	4510	0.11–0.55	CFRP
28	Lin and Liao.[97]	27	100–150	200–300	17.7–25.9	232	4170	0.138–0.413	CFRP
29	Liang et al. [98]	12	100–300	200–600	22.7–25.9	242	3591	0.167–0.501	CFRP
30	Mandal et al.[99]	9	102–105	200	30.7–54.5	26.1–47	575–784	0.8–2.6	CFRP,GFRP
31	Matthys et al.[100]	2	150	300	34.9	240–640	2650–3900	0.117–0.235	CFRP,HM-CFRP
32	Miyauchi et al.[101]	10	150	200–300	31.2–51.9	230.5	3481	0.11–0.33	CFRP
33	Modarelli et al.[102]	3	150	300	28.35–38.2	65–230	1700–3430	0.165–0.23	CFRP,GFRP
34	Owen.[103]	11	102–152 298	203–305 610	47.9–53 58.1	240–262	3900–4200	0.165–1.32	CFRP
35	Ongpeng[104]	2	180	500	27	231	3650	0.13–0.26	CFRP
36	Song et al.[105]	12	100–150	300–450	22.4–40.9	237	4073	0.13–0.39	CFRP
37	Shehata et al.[106]	6	150	300	25.6–29.8 61.7	235 240	3550 3900	0.165–0.33	CFRP
38	Shehata et al.[107]	4	150–225	300–450	34	235	3550	0.165–0.33	CFRP
39	Stanton and Owen[108]	5	152.5	305	49	238	4200	0.165–1.32	CFRP
40	Tamuzs et al.[109]	4	150	300	20.8–48.8	234	4500	0.34	CFRP
41	Theriault et al.[110]	5	51–304	102–608	18–37	27.6–230	552–3481	0.165–3.9	CFRP, GFRP
42	Valdmanis et al.[111]	6	150	300	40–44.3	234	4500	0.17–0.51	CFRP
43	Vincent et al.[112]	6	152	305	35.5–38	240	3800	0.117–0.234	CFRP
44	Picher et al.[113]	1	152	304	39.7	230	3400	0.33	CFRP
45	Piekarcky et al.[114]	2	47	112	55	110–113	1150–1420	0.51–0.82	CFRP
46	Rochette et al.[115]	7	100–150	200–300	42–43	13.6–230	230–3400	0.22–5.21	AFRP,CFRP
47	Rousakis et al.[8]	6	150	300	20.4–49.2	234	4493	0.17–0.51	CFRP
48	Saenz and Pantelides[116]	4	152	304	40.3–47.5	86.8	1220	1_2	CFRP
49	Santaros et al.[117]	3	150	300	15.3–28.1	230	3400	0.11–0.22	CFRP
50	Shahawy et al.[118]	9	152.5	305	19.4–49	207	3654	0.5–2.5	CFRP
51	Smith et al.[119]	4	250	500	35	210.52	3182	0.262	CFRP
52	Wang and Wu[120]	12	150	300	30.9–52.1	230–230.5	3482–3500	0.165–0.33	CFRP
53	Xiao and Wu[121]	27	152	305	33.7–55.2	105	1577	0.381–1.143	CFRP
54	Youssef et al.[46]	40	152.4–406.4	304.8–812.8	29.4–44.6	18.47–103.84	424.7–1246	1.168–7.267	CFRP, GFRP
55	Wu and Jiang[122]	38	150	300	20.6–36.7	230–242	3400–4059	0.167–0.668	CFRP
56	Nanni and Bradford[4]	17	150	300	35.6–36.3	72.59–127.5	2640–3240	0.215–2.16	AFRP,GFRP
57	Shao et al.[123]	2	152	305	40.2	72.4	2275	0.358–0.716	GFRP

(continued)

(continued)

Number	References	No. of specimens	Diameter (mm)	Height(mm)	Unconfined concrete strength range (MPa)	Mudul elasticity of FRP	FRP strength	Thickness of FRP	FRP type
58	Silva and Rodrigues[124]	7	150–250	300–750	29.6–31.1	26.1	575	2.6	GFRP
59	Zhang et al.[125]	1	150	300	34.3	240	3800	0.33	CFRP
60	Ahmad et al.[126]	2	102	203	39–50.5	48.3	2070	0.88	GFRP
61	Au and buykozturk[127]	1	150	375	24.2	26.1	575	1.2	GFRP
62	Bullo[128]	12	150	300	32.54	65–390	1700–3000	0.165–1.15	GFRP,HM-CFRP
63	Comert et al.[129]	2	150	300	39	65	1700	0.56	GFRP
64	Harries and Carey[130]	2	152	305	31.8	4.9	75	3_9	CFRP
65	Dai et al.[131]	9	152	305	39.2	78	2400	0.169–0.507	AFRP
66	Teng et al.[132]	6	152.5	305	39.6	80.1	1826	0.17–0.51	GFRP
67	Ozbakkaloglu et al.[133]	8	152	305	39 100–106	120	2900	0.4–0.6	AFRP
68	Suter and Pinzelli[134]	16	150	300	33.3–54	73–640	2300–3800	0.193–0.579	CFRP, AFRP, GFRP, HM-CFRP
69	Rousakis[3]	34	150	300	25.2–51.8 56.9–82.1	240–377	3900–4410	0.17–0.85	HM-CFRP
70	Wang and Wu[135]	18	70–194	210–582	23.98–51.63	118	2060	0.057–0.572	AFRP
71	Jiang and Teng[136]	8	152	305	33.1–45.9	80.1	1826	0.17–0.51	GFRP
72	Mirmiran et al.[137]	13	152.5	305	29.8–31.2	55.85	1800	0.275–1.376	GFRP
73	Yan et al.[138]	1	305	610	15	86.9	1220	1	CFRP
74	Li et al.[139]	1	152.4	305	45.6	70	3000	0.4	GFRP
75	Watanabe et al.[140]	9	100	200	30.2	73–637	2452–3432	0.14–0.668	CFRP, AFRP, HM-CFRP
76	Wong et al.[141]	4	152.5	305	36.5–46.7	80.1	1826	0.34–0.51	GFRP
77	Micelli[142]	1	102	204	32	72	1520	0.35	GFRP,CFRP
78	Hosotani et al.[143]	2	200	600	41.7	392–439	2943–3972	0.652–0.676	CFRP
79	Mastrapa[144]	6	152.5	305	29.8–37.2	55.85	1800	0.33–2.311	GFRP
80	Wu et al.[147-145]	22	100–150	200–300	23–46.4 78.5–102.2	73–540 120	1500–3400, 2900	0.167–0.354	CFRP, AFRP, GFRP, HM-CFRP,AFRP
81	Vincent et al.[148]	24	152	305	49.4 59.1–102.5	120–240	2900–3900	0.6	CFRP
82	Ilki et al.[149]	12	150	300	6.2	230	3430	0.165–0.99	CFRP
83	Lin, H.J., Chen[150]	10	120	240	32.7	32.9–157.54	743.9–770	0.5–1.8	GFRP,CFRP
84	Howie[151]	12	152	305	38.6	70.6–95.7	755–1352	0.305–1.22	GFRP,CFRP
85	Issa[152]	9	150	300	30.5	230	4100	0.1220.366	CFRP
86	Lin and Liao[153]	6	100	200	23.9	22.46–23.83	403.1–455.4	1.84–3.89	CFRP

(continued)

(continued)

Number	References	No. of specimens	Diameter (mm)	Height(mm)	Unconfined concrete strength range (MPa)	Mudul elasticity of FRP	FRP strength	Thickness of FRP	FRP type
87	Mivauchi et al.[154]	8	100–150	200–300	23.6–26.3 109.5	230.5–240	3481–3900	0.11–0.33	CFRP
88	Abdollahi et al.[155]	5	150	300	14.8–41.7	26.49	537	0.508–2.032	GFRP
89	Almusallam[156]	12	150	300	47.7–50.8 60–107.8	26 76	540 2200	1.3–3.9 62.4–125.2	CFRP GFRP
90	Wang and Zhang[157]	2	150	450	47.3–51.1	118	2060	0.572	
91	Parketal[158]	12	150	300–450	32–54	39.59–56.99	321–607	1–5	GFRP
92	Saafi et al.[159]	6	152	435	35	32–415	450–3700	0.11–1.6	GFRP
93	Aire et al.[160]	5	150	300	69	240	3900	94–217	CFRP
94	Chikh et al.[161]	2	160	320	61.8	240	3900	62.68–93.19	CFRP
95	Green[162]	2	152	305	59	76–240	2200–3900	69.9–77.3	CFRP, GFRP
96	Aire et al.[163]	5	150	300	69	76	2200	94–199	GFRP
97	Benzaid et al.[164]	3	160	320	56.7	76	2200	74–95.5	GFRP
98	Mandal and Fam[165]	18	100	200	67.0–80.6	76–240	2200–3900	81.3–104.6	CFRP, GFRP
99	Ozbakkaloglu et al.[166]	69	74–152	62–111.6	59.0–110.1	76–377	2200–4410	0.12–0.7	CFRP, HM-CFRP
100	Valdmanis et al.[167]	3	150	300	61.6	240.00	3900.00	0.17–0.51	CFRP
101	Xiao et al.[168]	12	152	305	70.8–111.6	240.00	3900.00	0.11–3	CFRP
102	Cao et al.[169]	3	150	300	69.33	240.00	3900.00	1–0.5-1.4	CFRP
103	Vincent[170]	3	152	305	110.3	120–240	2900–3900	0.8	AFRP
104	Oliveira et al.[171]	66	50–100	100–200	112–204	76–240	2200–3900	0.13–0.66	CFRP-GFRP
105	Ostrowski[172]	3	150	300	80.04–92.5	240.00	3900.00	0.12–0.7	CFRP
106	Touhari et al.[173]	18	160	320	61.5–61.7	76–240	2200–3900	0.13–1.76	CFRP, GFRP

Appendix 2

Notation

D	Diameter(mm)
E_f	Modulus of elasticity of FRP
f_{c_0}	Unconfined ultimate concrete strength(MPa)
f_{cc}	Confiend ultimate compressive strength (MPa)
F_f	Tensile strength of FRP
$f_{l,a}$	Confining pressure(MPa)
H	Height(mm)
k_ε	Effective strain factor
tj	FRP twist thickness (mm)
β_3, γ_3 , δ_3	Optimal values obtained from the genetic optimization algorithm
$\varepsilon_{h,rup}$	Actual strain of FRP rupture
ε_{frp}	Ultimate tensile strain of FRP
ε_0	Unconfines concrete strain
η_3, θ_3, λ_3, ξ_3	Optimal values obtaines from the genetic optimization algorithm
ρ_ε	Strain ratio factor
ρ_k	Stiffness ratio coefficient
Φ_3	Optimal values obtaines from the genetic optimization algorithm